

hep-ph/0203052

FTUAM-02-06

IFT-UAM/CSIC-02-04

Corrections to the fluxes of a Neutrino Factory

A. Broncano^{a,1}, O. Mena^{a,2}^a Dept. de Física Teórica, Univ. Autónoma de Madrid, 28049 Spain

Abstract

In view of their physics goals, future neutrino factories from muon decay aim at an overall flux precision of $\mathcal{O}(1\%)$ or better. We analytically study the QED radiative corrections to the differential distributions of muon decay. The $\mathcal{O}(1\%)$ corrections to the energy and angular distributions for electrons are obtained in the “leading log” approximation, while the exact corrections are considered for neutrinos. Kinematic uncertainties due to the divergence of the muon beam are considered as well. The resulting corrections to the neutrino flux turn out to be of order $\mathcal{O}(0.1\%)$, safely below the required precision.

¹alicia@delta.ft.uam.es²mena@delta.ft.uam.es

1 Introduction

Results on neutrino oscillations from Superkamiokande [1] and SNO [2] provide a compelling evidence for neutrino masses, constituting the first strong indication of Physics beyond the Standard Model. Much is still unknown, though, regarding fundamental issues such as the absolute neutrino mass scale, the possible Majorana character of neutrino fields, the ordering of their mass eigenstates with respect to charged lepton eigenstates, or the possible existence of leptonic CP violation and its tantalizing relationship to baryogenesis. In this situation one could argue that the subject of lepton flavor physics is at its exciting infancy, and to obtain rough answers to those questions could be a sufficient goal at present, postponing any aim at a precise determination of the involved parameters. Nevertheless, some of those questions prerequisite precision: for instance the study of CP violation rests upon a precise knowledge of the angles in the neutrino mixing matrix.

In a more general way and much as for the quark sector, it is necessary to know accurately the values of the masses and mixing parameters in the lepton sector, as a first step to unravel the flavor puzzle. And what does precision means, quantitatively?. For instance, with which precision is it desirable to determine the values of the leptonic mixing angles in order to discriminate between models for neutrino masses? Clearly no definite answer can be given to such question, but as an indication it has been argued [4] that a 10% – 1% precision in the knowledge of, say, $\sin^2 2\theta_{atm}$ would result in significant advance¹. It is not impossible to envisage such a precision. In resume, we are simultaneously entering a discovery and a precision era in neutrino physics. With the bonus that the extraction of physical conclusions will not be necessarily hindered by large theoretical errors, as it happens in the quark sector due to QCD long distance contributions.

A quest for precise physics answers evidently requires an effort in precision on the experimental conditions, and on the knowledge of the neutrino flux to start with. Several experiments using neutrino beams from particle accelerators such as K2K, MINOS and OPERA [3] will take data in the next few years. Their reach will be limited by the use of conventional neutrino beams produced from a charged pion source. The decay $\pi^+ \rightarrow \mu^+ \nu_\mu$ ($\pi^- \rightarrow \mu^- \bar{\nu}_\mu$) produces a ν_μ beam with a $\mathcal{O}(1\%)$ component of ν_e from kaon decays. The ν_e contamination limits the precision of the flux measurements, resulting in an error of 7% for K2K, while MINOS reduces it to 2% [3]. A further step forward could be provided by the so-called superbeams which, although based on the same traditional beams, can achieve better precision thanks to the much higher statistics. It has been argued, for example, that by working at energies below the threshold of kaon production, the ν_e flavor contamination could be reduced, with the overall figure of merit for precision in the flux measurements limited to $\mathcal{O}(1\%)$ [5, 6].

¹ θ_{atm} denotes the mixing angle dominantly responsible for the atmospheric oscillations, denoted by θ_{23} in the by now standard parameterization [17]

A major advance should come from a neutrino factory from muon decays, aiming at both fundamental discoveries and $\mathcal{O}(1\%)$ precision measurements. Present projects consider the production of very intense muon sources of about 10^{20} muons per year [7]. Neutrino beams originate from the decay of high-momentum muons along the straight sections of a storage ring. The beam produced presents a precisely known neutrino content: 50% muon neutrinos and 50% electron antineutrinos if a μ^- beam is used, and 50% muon antineutrinos and 50% electron neutrinos if a μ^+ beam is used. The resulting ν fluxes are expected to be known with a precision better than 1% [8]. It is necessary to ensure that any possible corrections and sources of errors are controlled at that level. In this work, we study two effects: the contribution of QED one-loop corrections to muon decay and the divergence of the muon beam.

Radiative corrections to the electron differential distribution in $\mu^- \rightarrow e^- + \bar{\nu}_e + \nu_\mu$ were calculated long ago [9] resulting in a correction of $\mathcal{O}(1\%)$. In our work, we discuss the origin of this large effect by computing the electron energy and angular distribution within the “leading log” approximation, in which the $\mathcal{O}(\alpha)$ correction is restricted to the dominant terms, proportional to $\ln(\frac{m_\mu}{m_e})$. Electron angular distributions are used in neutrino factories to measure the muon polarization and, from this, the muon beam energy distribution [10].

First order QED corrections to the neutrino angular and energy distribution are also computed. No large logarithmic corrections are present in this case, and the $\mathcal{O}(\alpha)$ contributions are exactly evaluated in the limit $m_e = 0$. The correction to the (massive) neutrino spectra from unpolarized muons has been calculated in [12]. In our analysis we set $m_\nu = 0$ and include muon polarization, relevant for neutrino factory measurements.

The second subject addressed in this paper is that of the muon beam divergence, one of the basic properties that can bias the predicted neutrino spectra. We explore the error induced in the neutrino distributions at the far site due to the systematic uncertainty on the angular divergence, and compare ours results with previous ones in which this effect was not included [28].

The paper is organized as follows. In section 2 we recall the tree-level angular distributions. Section 3 discusses the leading logarithmic QED corrections. In section 4 the exact one-loop corrected formulae are given, with subsections 4.1 and 4.2 specializing in the contribution from virtual and real photons, respectively, and subsection 4.3 in the soft photon limit and cancellation of infrared divergences. Section 5 accounts for the corrections due to the beam divergence.

2 General definitions

In the muon rest-frame, the angular distributions of the neutrinos produced in the decay $\mu^- \rightarrow e^- + \nu_\mu + \bar{\nu}_e$, Fig. 1a, are computed from the muon decay rate:

$$d\Gamma_0 = \frac{1}{2m_\mu} 64 G_F^2 |M_0(p_\mu; p_e, p_{\bar{\nu}_e}, p_{\nu_\mu})|^2 d\Phi_3(p_\mu; p_e, p_{\bar{\nu}_e}, p_{\nu_\mu}), \quad (1)$$

where $|M_0(p_\mu, p_e, p_{\bar{\nu}_e}, p_{\nu_\mu})|^2$ is the averaged squared amplitude obtained from the Feynmann diagram at tree level. For polarized muons:

$$|M_0(p_\mu; p_e, p_{\bar{\nu}_e}, p_{\nu_\mu})|^2 = [(p_\mu - m_\mu s) p_{\bar{\nu}_e}] (p_e p_{\nu_\mu}), \quad (2)$$

where s is the four-spin. For unpolarized muons $s = 0$.

$d\Phi_3$ is the three-body phase-space. In general, the n-body phase space is defined by :

$$d\Phi_n(P; p_1, \dots, p_n) = (2\pi)^4 \delta(P - p_1 - \dots - p_n) \prod_{i=1}^n \frac{d^3 \mathbf{p}_i}{2p_i^0} \frac{1}{(2\pi)^3}. \quad (3)$$

Differential distributions of decay products are obtained integrating over the phase space of the remaining decay particles,

$$\frac{d^2 N}{dx d\cos\theta} = F^{(0)}(x) + J^{(0)}(x) \mathcal{P}_\mu \cos\theta, \quad (4)$$

where x denotes the scaled energy, $x = 2E_{e,\nu}/m_\mu$ and \mathcal{P}_μ is the average over polarization of the initial state muon along the beam direction. θ is the angle between three-momentum of the emitted particle and the muon spin direction and m_μ is the muon mass. The normalized functions $F^{(0)}$ and $J^{(0)}$, in the limit $m_e = 0$, read [16]:

$$\begin{aligned} F_e^{(0)}(x) &= x^2(3 - 2x), & J_e^{(0)}(x) &= x^2(1 - 2x), \\ F_{\nu_\mu}^{(0)}(x) &= x^2(3 - 2x), & J_{\nu_\mu}^{(0)}(x) &= x^2(1 - 2x), \\ F_{\bar{\nu}_e}^{(0)}(x) &= 6x^2(1 - x), & J_{\bar{\nu}_e}^{(0)}(x) &= 6x^2(1 - x). \end{aligned} \quad (5)$$

The QED radiative corrections to the above formulae will be computed in what follows using the Fermi effective lagrangian for four Fermi weak corrections, as all pure QED divergences do cancel in this approximation. There are three diagrams containing a photon loop: the exchange of the virtual photon between the muon and the electron legs, Fig. 1b, and lepton propagator corrections, Figs. 1c, 1d. They correct the invariant amplitude of the muon decay as follows:

$$-i M = \frac{G_F}{\sqrt{2}} \{ \bar{u}(p_e) \Gamma_\sigma u(p_\mu) \} \{ \bar{u}(p_{\nu_\mu}) \gamma^\sigma (1 - \gamma_5) v(p_{\bar{\nu}_e}) \}. \quad (6)$$

Γ_σ is the corrected $\mu - e$ vertex:

$$\Gamma_\sigma = \gamma_\sigma(1 - \gamma_5) + \Gamma_\sigma^a + \Gamma_\sigma^{c,d}, \quad (7)$$

where Γ_σ^b results from the diagram in Fig. 1b and $\Gamma_\sigma^{c,d}$ from those in Figs. 1c, 1d. Ultra-violet (UV) divergences cancel when the three diagrams are summed up. Their infrared singularities (IR) are cancelled with the soft contributions of the bremsstrahlung diagrams in Figs. 1e, 1f. The overall effect is expected to be of $\mathcal{O}(\frac{\alpha}{\pi}) \sim \mathcal{O}(0.1\%)$, although in some cases, the correction can be enhanced up to the percent level by logarithmic factors. This will be discussed in the next section.

3 Leading logarithms in QED radiative corrections

For the e^- properties in muon decay, the most important QED radiative corrections stem from the physics of collinear photons. Electrons are much lighter than muons and radiate more. As a consequence, the leading radiative effects come from processes where photons are attached to electrons. Indeed, the emission of multiple collinear photons from the electron leg gives contributions of the form $(\frac{\alpha}{\pi} \ln(\frac{s}{m_e}))^n$, where s is the typical energy scale of the process, i.e. m_μ for muon decay. In the $m_e = 0$ limit, these logarithms can be potentially large.

Although the exact corrections to the e^- differential distributions have been computed at $\mathcal{O}(\alpha)$, we will in practice consider just the terms in $\frac{\alpha}{\pi} \ln(\frac{m_\mu}{m_e})$: for the electrodynamic corrections considered here this is a highly accurate approximation. However, the correction to the neutrino distributions turns out to be independent of m_e and no mass singular logarithms are present as it occurs for the muon lifetime. In both cases, the integration over the part affected by QED corrections, namely, the photon-electron system, cancels all the terms involving mass singularities [22]. It must be remarked that this only occurs once the virtual and bremsstrahlung contributions at $\mathcal{O}(\alpha)$ are added.

In the next subsection we discuss the origin of the “leading logs”. As we shall see, the relation between the observed decay width and the bare differential decay width $d\Gamma_B$ takes the form

$$d\Gamma_{obs} = d\Gamma_B + \frac{\alpha}{2\pi} \ln\left(\frac{m_\mu^2}{m_e^2}\right) F[d\Gamma_B] + \frac{\alpha}{2\pi} G, \quad (8)$$

where F is an explicit functional of $[d\Gamma_B]$. The coefficient G does not contain logarithms of the form $\frac{\alpha}{\pi} \ln(\frac{m_\mu}{m_e})$. The “leading log” approximation seriously deteriorates at the edges of the kinematically allowed regions where singularity appears. This behavior is a general feature of QED corrections and is related to photon emission when the photon is simultaneously collinear and soft. In subsection 3.2, we show that this divergence takes the form of double singular logarithms and we discuss their exponentiation which gets rid of it.

3.1 “Leading log” approximation to the e^- distribution

Muons at a neutrino factory are completely polarized in their own rest frame. Boosting the system to the laboratory frame, the muon momentum and spin loose their collinearity and the longitudinal polarization is generally less than 1. For the typical energies of the neutrino factory, the average muon polarization is $\mathcal{P}_\mu \sim 0.2$ [11]. The distribution of electrons at the neutrino factory serves as a muon polarimeter because the dependence of the angle between the muon spin direction and the electron trajectory is proportional to the muon polarization. Using this property, the muon polarization is expected to be measured with a precision of $\mathcal{O}(1\%)$ [10]. Any possible source of error at this level must be taken into account. In this subsection we consider the leading correction introduced in the electron distribution by QED radiative corrections.

Mass singularities arise from the collinear emission of photons by a lepton in an external leg. For muon decay, it occurs in the limit $m_e \rightarrow 0$ when the electron emits a collinear photon, Fig. 1f. In this case, the propagator of the electron $1/(p_e k)$ vanishes, where p_e (k) is the electron (photon) momentum. To compute the leading logarithm it suffices to set $m_e^2 = 0$ and $k^2 = 0$ in the numerator of the bremsstrahlung amplitude and take k to be proportional to p_e :

$$p_e^\mu = z P^\mu, \quad k^\mu = (1 - z) P^\mu, \quad (9)$$

where $0 < z < 1$ since $P = p_e + k$ is the momentum of the virtual electron before photon radiation.

Hence, the squared amplitude of the collinear emission process reads:

$$|M_L|^2 = |M_0(p_\mu, z p_e, p_{\bar{\nu}_e}, p_{\nu_\mu})|^2 \frac{\alpha}{2\pi} \frac{1}{(p_e k)} \frac{1+z^2}{1-z}, \quad (10)$$

where $|M_0(p_\mu, z p_e, p_{\bar{\nu}_e}, p_{\nu_\mu})|^2$ is the tree level amplitude given in eq. (2), with an emitted virtual electron of momentum $z p_e = P$. To obtain the electron distribution in the muon rest frame, we must integrate eq. (10) over the neutrinos and photon phase space:

$$\begin{aligned} \int \frac{d^3 \mathbf{k}}{(2k^0)} \int |M_L|^2 \frac{d^3 \mathbf{p}_{\bar{\nu}_e}}{2p_{\bar{\nu}_e}^0} \frac{d^3 \mathbf{p}_{\nu_\mu}}{2p_{\nu_\mu}^0} &= \frac{\alpha}{(2\pi)^2} \int \frac{d^3 \mathbf{k}}{(2k^0)} A(z) \\ &= \frac{\alpha}{2\pi} \int_{\varphi_{\min}}^1 \frac{d \cos \varphi}{(1 - \omega \cos \varphi)}, \int_x^1 \frac{dz}{z} \frac{1+z^2}{1-z} A(z) \\ &= \frac{\alpha}{2\pi} \ln \left(\frac{m_\mu}{m_e^2} \right) \int_x^1 \frac{dz}{z} \frac{1+z^2}{1-z} A(z), \end{aligned} \quad (11)$$

where $\omega = |\mathbf{p}_e|/E_e$, φ is the angle between \mathbf{k} and \mathbf{p}_e and

$$A(z) \equiv \frac{m_\mu^2}{4} x^2 z [(3 - 2 z x) - s \cos \theta (1 - 2 z x)] \quad (12)$$

is the integrated amplitude with $x = 2E_e/m_\mu$. The lower limit $z > x$ arises from the requirement that the maximum energy of the virtual electron be larger than the detected electron energy E_e .

In addition to the mass singularity $m_e \rightarrow 0$, eq. (11) contains a singularity for $z = 1$, i.e. when the photon radiated has zero energy (soft photon). This is an infrared singularity which must be canceled by virtual photon corrections where no photon is radiated. Hence, the photon exchange diagrams subtract from eq. (11) a term proportional to $\delta(1 - z)$ [25]. Working in the physical gauge where the photon enjoys only transverse polarizations, the $\mu - e$ vertex correction, Fig. 1b, does not give “leading log” contributions [26]. The factor preceding the delta function is extracted only from the electron self-energy diagram, Fig. 1d, since $m_e \ll m_\mu$. Taking into account the virtual photon terms, the corrected electron distribution has the following form:

$$\begin{aligned} \frac{d^2 N_e^{\text{LL}}}{dx d \cos \theta} &= \frac{d^2 N_e^{(0)}}{dx d \cos \theta} \\ &+ \frac{\alpha}{2\pi} \ln \left(\frac{m_\mu^2}{m_e^2} \right) \int_x^1 \frac{dz}{z} \left(\frac{1+z^2}{(1-z)_+} + \frac{3}{2} \delta(1-z) \right) A(z), \end{aligned} \quad (13)$$

where the function $1/(1-z)_+$ is defined as having no singularities [27]:

$$\frac{1}{(1-z)_+} \equiv \lim_{\epsilon \rightarrow 0} \left\{ \frac{1}{(1-z)} \theta(1-z-\epsilon) - \delta(1-z) \int_0^{1-\epsilon} dy \frac{1}{1-y} \right\}. \quad (14)$$

The factor $-3/2$ of the delta function can also be worked out considering that the muon lifetime does not contain mass logarithms. Therefore, when the corrected electron distribution is integrated over θ and x , the term of $\mathcal{O}(\alpha)$ must give zero contribution to the lifetime. Imposing that condition on the collinear photon emission results, eq. (11), we obtain the same factor preceding the delta function.

The leading correction follows then from integrating eq. (13) over z and averaging over the muon spin:

$$\begin{aligned} \frac{d^2 N_{\nu_\mu}}{dx d \cos \theta} &= F_e^{(0)}(x) + J_e^{(0)} \mathcal{P}_\mu(x) \cos \theta \\ &+ \frac{\alpha}{2\pi} \ln \left(\frac{m_\mu^2}{m_e^2} \right) [F_e^{(LL)}(x) + J_e^{(LL)}(x) \mathcal{P}_\mu \cos \theta], \end{aligned} \quad (15)$$

where $F_e^{(0)}(x), J_e^{(0)}(x)$ are given in (5) and

$$\begin{aligned} F_e^{(LL)}(x) &= 2F_e^{(0)}(x) \ln \left(\frac{1-x}{x} \right) + 2x(1-2x^2) + \frac{5}{6} + \frac{8z^3}{3}, \\ J_e^{(LL)}(x) &= 2J_e^{(0)}(x) \ln \left(\frac{1-x}{x} \right) - 4x^2 - \frac{1}{6} + \frac{8z^3}{3}. \end{aligned} \quad (16)$$

The “leading log” contributions will arise solely from the larger terms in eq. (16). Discarding all other terms, it follows a correction proportional to the tree level distributions

$$\frac{d^2 N_e}{dx d \cos \theta} = [F_e^{(0)}(x) + J_e^{(0)} \mathcal{P}_\mu(x) \cos \theta] \left(1 + \frac{\alpha}{\pi} \psi(x) \right), \quad (17)$$

where

$$\psi(x) \equiv \ln \left(\frac{m_\mu^2}{m_e^2} \right) \ln \left(\frac{1-x}{x} \right) \quad (18)$$

contains the leading logarithms and diverges for $x \rightarrow 1$.

Fig. 2 compares the tree level forward distribution with those corrected within the “leading log” approximation and with the exact $\mathcal{O}(\alpha)$ formulae [9], given in appendix C. The effect is in both cases of $\mathcal{O}(1\%)$, except at the upper part of the allowed energy range where it is larger, see Fig. 3. At the kinematical edge, the “leading log” deteriorates, since we have not considered the function G , defined as having no mass singularities, which also diverges for $x \rightarrow 1$. In the next subsection we will study the origin and cancellation of the end-point singularity.

3.2 End-point singularity

The end-point singularity originates when the phase space for the emission of real photons shrinks to zero and does not compensate the IR infinities of the virtual photons. Hence, it is essentially an IR problem and a signal of a failure of the perturbative treatment at the end-point region $x \rightarrow 1$. We summarize here the solution to this problem discussed in the literature [23] for the corrected e^- distribution. After that, we study the form of the divergence for the neutrino distributions, following as a guideline the solution found for the electron.

For $x \rightarrow 1$ and $m_e \rightarrow 0$, the exactly corrected electron differential distribution, diverge as two singular logarithms:

$$\frac{d^2 N_e}{dx d \cos \theta} = [F_e^{(0)}(x) + J_e^{(0)} \mathcal{P}_\mu(x) \cos \theta] \left(1 + \frac{\alpha}{\pi} \ln(1-x) \right) \left[\ln \left(\frac{m_\mu^2}{m_e^2} \right) - 2 \right]. \quad (19)$$

The IR divergences stem from soft-photons on the limit $k \rightarrow 0$. Then, the solution proposed to control the double divergence of eq. (19) is to consider multiple soft-photon emission. In [24] it was shown that the contribution of soft photons at all orders in α gives rise to the exponentiation of the double singularity:

$$\frac{d^2 N_e}{dx d \cos \theta} = [F_e^{(0)}(x) + J_e^{(0)} \mathcal{P}_\mu(x) \cos \theta] e^{\frac{\alpha}{\pi} \ln(1-x) \left[\ln \left(\frac{m_\mu^2}{m_e^2} \right) - 2 \right]} \quad (20)$$

The exponentiation method can only be applied very close to the end-point of the e^- spectrum. The application to the whole range $0 < x < 1$ results in terms of $\mathcal{O}(\alpha^2)$ and higher when the exponential is expanded, which would go beyond the “leading log” approximation considered here.

Consider now the procedure for the neutrino distributions. We shall see explicitly in the next section how, when the soft photon limit is applied to the $\mathcal{O}(\alpha)$ diagrams in Figs. 1b-1d, only IR singular terms remain for both virtual and photon emission. These two sets of IR divergences cancel each other, and a safe IR correction results.

We anticipate that the soft-photon correction for both ν_μ and $\bar{\nu}_e$ is proportional to the tree level amplitude and, in the limits $x \rightarrow 1$ and $m_e \rightarrow 0$, it has the form:

$$\frac{d^2 N_\nu}{dx d \cos \theta} = [F_\nu^{(0)}(x) + J_\nu^{(0)} \mathcal{P}_\mu(x) \cos \theta] \left(1 - \frac{\alpha}{2\pi} \ln^2(1-x) \right). \quad (21)$$

Then, at the end-point, for each soft virtual photon and each soft real photon we get a $\ln^2(1-x)$ term, which multiplies the tree level amplitude. If there are n soft virtual photons and n soft real photons, there are n double logarithms with an additional symmetry factor of $1/n!$. Therefore, the correction to the neutrino distribution at all orders in α is obtained summing over n :

$$\frac{d^2 N_\nu}{dx d \cos \theta} = [F_\nu^{(0)}(x) + J_\nu^{(0)} \mathcal{P}_\mu(x) \cos \theta] e^{-\frac{\alpha}{2\pi} \ln^2(1-x)}. \quad (22)$$

As a result of the evaluation of infrared divergences at all orders, double logarithms are exponentiated, which ensures a non-divergent behavior of the distributions. The exponentiation is only valid for a small region $x \rightarrow 1$. For lower x , we must include all the terms of the exact corrections, computed in the next section.

4 Exact QED Corrections ($m_e = 0, m_\nu = 0$)

The radiative corrections to the neutrino angular and energy distributions are expected to be of $\mathcal{O}(\frac{\alpha}{\pi}) \sim \mathcal{O}(0.1\%)$, that is, once it is integrated over the variables affected by QED corrections, we do not expect any “leading-log” correction of the form $\frac{\alpha}{\pi} \ln(\frac{m_\mu}{m_e})$. The absence of QED corrections in the neutrino legs also ensures that no terms in $\log(\frac{m_\mu}{m_\nu})$ will appear. Hence, we set $m_\nu = 0$ from the beginning of the calculation but retain $m_e \neq 0$ until loop and photon emission diagrams are summed up, which cancels IR and mass singularities.

4.1 Photon loops

The computation of the diagrams in Figs. 1b-1d, is summarized in Appendix A. The cancellation of UV divergences is detailed there. The remaining terms contain IR

divergences that will be regularized here by a finite photon mass λ . As a result of adding up the contributions from all virtual photon diagrams, the $\mu - e$ vertex (7) is corrected at order α as follows:

$$\begin{aligned}\Gamma_\sigma &= (1 - \gamma_5) - \frac{\alpha}{2\pi} [g_L^S \gamma_\sigma (1 - \gamma_5) + g_R^S \gamma_\sigma (1 + \gamma_5) \\ &\quad + g_L^V p_{1\sigma} (1 - \gamma_5) + g_R^V p_{2\sigma} (1 + \gamma_5)],\end{aligned}\quad (23)$$

where $g_{L,R}^{S,V}$ are listed in the appendix A. The function g_L^S contains the IR divergences while the rest of the “ g ” functions are finite.

The interference of loop diagrams with the tree level amplitude yields the $\mathcal{O}(\alpha)$ correction to the decay rate

$$d\Gamma_v = \frac{1}{2m_\mu} 64 G_F^2 |M_V|^2 d\Phi_3(p_\mu; p_e, p_{\bar{\nu}_e}, p_{\nu_\mu}), \quad (24)$$

where $|M_V|^2$ for unpolarized muons is given by:

$$|M_V|^2 = |M_0|^2 - \frac{\alpha}{2\pi} [H_0|M_0|^2 + H_1(p_\mu p_{\bar{\nu}_e})(p_\mu p_{\nu_\mu}) + H_2(p_e p_{\bar{\nu}_e})(p_e p_{\nu_\mu}) + H_3(p_{\bar{\nu}_e} p_{\nu_\mu})], \quad (25)$$

and the “H” functions are defined as

$$H_0 = 2 g_L^S, \quad H_1 = 2 m_e g_L^V, \quad H_2 = 2 m_\mu g_R^V, \quad H_3 = \frac{m_\mu m_e}{2} g_R^S. \quad (26)$$

In eq. (25) we have followed the same notation used in [18] for the QCD corrections to the lepton spectra in the decay $t \rightarrow b + l + \nu_l$. We use their techniques to parameterize the three body phase space $d\Phi_3(p_\mu; p_e, p_{\bar{\nu}_e}, p_{\nu_\mu})$ in terms of the Euler angles (α, θ, γ) describing the orientation of the outgoing particles, the scaled neutrino energy $x_\nu = E_\nu/m_\mu$ and the variable $y = \frac{(p_{\bar{\nu}_e} + p_{\nu_\mu})^2}{m_\mu^2}$:

$$d\Phi_3(x, y) = \frac{1}{(4m_\mu)^2} \frac{1}{(2\pi)^5} dx dy d\alpha d\gamma d\cos\theta. \quad (27)$$

The functions “H” and the scalar products appearing in eq. (25) are functions of y , $x_{\bar{\nu}_e}$, x_{ν_μ} . For instance, for $m_e = 0$ the tree level amplitude reads:

$$\begin{aligned}|M_0(x_{\bar{\nu}_e}, y)|^2 &= \frac{(m_\mu)^2}{4} x_{\bar{\nu}_e} (1 - x_{\bar{\nu}_e}), \\ |M_0(x_{\nu_\mu}, y)|^2 &= \frac{(m_\mu)^2}{4} (x_{\nu_\mu} - y) (1 - y - x_{\nu_\mu}),\end{aligned}\quad (28)$$

where the following relation has been used:

$$1 = x_{\bar{\nu}_e} + x_{\nu_\mu} - y. \quad (29)$$

4.2 Real photon emission

The contribution from real photon emission, Figs. 1e, 1f, is given by

$$d\Gamma_r = \frac{1}{2m_\mu} 64 G_F^2 |M_R|^2 d\Phi_4(p_\mu; p_e, p_{\bar{\nu}_e}, p_{\nu_\mu}, k), \quad (30)$$

where the amplitude $|M_R|^2$ has the following expression:

$$|M_R|^2 = \frac{\alpha}{2\pi} \left[\frac{A}{(p_\mu k)^2} + \frac{B}{(p_e k)^2} - \frac{C}{(p_\mu k)(p_e k)} \right], \quad (31)$$

and the numerators for unpolarized muons read:

$$\begin{aligned} A &= p_\mu^2 [(p_\mu p_{\bar{\nu}_e})(p_e p_{\nu_\mu}) - (kp_{\bar{\nu}_e})(p_e p_{\nu_\mu}) - (p_\mu k)(kp_{\bar{\nu}_e})(p_e p_{\nu_\mu})] \\ B &= p_e^2 [(p_\mu p_{\bar{\nu}_e})(p_e p_{\nu_\mu}) + (p_\mu p_{\bar{\nu}_e})(kp_{\nu_\mu}) - (p_\mu p_{\bar{\nu}_e})(p_e k)(kp_{\nu_\mu})] \\ C &= (p_\mu p_e) [2(p_\mu p_{\bar{\nu}_e})(p_e p_{\nu_\mu}) + (p_\mu p_{\bar{\nu}_e})(kp_{\nu_\mu}) - (kp_{\bar{\nu}_e})(p_e p_{\nu_\mu})] \\ &\quad + (p_e k) [(p_\mu p_{\bar{\nu}_e})(p_e p_{\nu_\mu}) + (p_\mu p_{\bar{\nu}_e})(p_\mu p_{\nu_\mu}) - (p_\mu p_{\bar{\nu}_e})(kp_{\nu_\mu})] \\ &\quad - (p_\mu k) [(p_\mu p_{\bar{\nu}_e})(p_e p_{\nu_\mu}) + (p_e p_{\bar{\nu}_e})(p_e p_{\nu_\mu}) - (kp_{\bar{\nu}_e})(p_e p_{\nu_\mu})]. \end{aligned} \quad (32)$$

Terms of order k^2 are not included in eq. (32), since they vanish in the limit of massless photons.

To obtain the exactly corrected neutrino spectra, we must integrate over the photon and electron momenta. The following decomposition of the four-body phase space [17] is useful:

$$d\Phi_4(p_\mu; p_e, p_{\bar{\nu}_e}, p_{\nu_\mu}, k) = m_\mu^2 dM^2 d\Phi_3(p_\mu; P, p_{\bar{\nu}_e}, p_{\nu_\mu}) d\Phi_2(P; p_e, k), \quad (33)$$

where $M^2 \equiv P^2$ is the invariant mass of the electron-photon system. The integration over $[dM^2 d\Phi_2(P; p_e, k)]$ is a difficult task and we follow the method detailed in [18] to perform it. The amplitude can then be written as a function of x and y and the integration over the remaining decay particles is performed parametrizing $d\Phi_3(p_\mu; P, p_{\bar{\nu}_e}, p_{\nu_\mu})$ as in eq. (27).

4.3 Soft photon limit and IR cancellation

Before continuing with the discussion of the exact corrections, let us consider their soft photon limit, i.e. $k \rightarrow 0$, in order to illustrate the discussion about the end-point singularities mentioned in the previous section. As stated there, only IR singular terms of virtual and real photon diagrams remain in this limit. When soft virtual and soft real photon contributions are added up, all $\mathcal{O}(\alpha)$ IR singularities are canceled.

In this limit, the $\mathcal{O}(k)$ terms in the virtual photon diagrams, Figs. 1b-1d, are neglected and eq. (23) reduces to:

$$\Gamma_\sigma^{SP} = \gamma_\sigma (1 - \gamma_5) (1 - \frac{\alpha}{2\pi} g_L^S), \quad (34)$$

where g_L^S contains all IR divergent term of the form:

$$\ln \left(\frac{\lambda^2}{m_e m_\mu} \right), \quad (35)$$

The corrected squared amplitude in eq.(25) is simplified to :

$$|M_V^{\text{SP}}|^2 = \left(1 - \frac{\alpha}{2\pi} H_0(x, y) \right) |M_0|^2, \quad (36)$$

Consider now the diagrams containing real photon emission, Figs. 1e,1f . Only terms of order $\mathcal{O}(k^{-2})$ remain in the soft photon limit. They contain all IR divergent contributions from bremsstrahlung . The squared amplitude in eq.(32) reduces to:

$$|M_r^{\text{SP}}|^2 = 32 \frac{\alpha}{2\pi} \left[\frac{p_\mu^2}{(p_\mu k)^2} + \frac{p_e^2}{(p_e k)^2} - \frac{2(p_\mu p_e)}{(p_\mu k)(p_e k)} \right] |M_0|^2. \quad (37)$$

The divergences in eq. (36) cancel when added with the soft bremsstrahlung part. However, eq. (37) must be previously integrated over the photon-electron phase space in order to reduce the contribution to a three-body problem. The integral is performed introducing a finite photon mass λ resulting in a correction:

$$\frac{\alpha}{2\pi} J_0(x, y) |M_0(p_\mu, P, p_{\bar{\nu}_e}, p_{\nu_\mu})|^2, \quad (38)$$

where now the IR singularities are contained in the function $J_0(x, y)$ and which exactly cancel those in eq.(35). By the same token, all logarithmic singularities appearing in the $m_e \rightarrow 1$ limit do cancel.

The resulting function in λ -independent:

$$K_0(x, y) \equiv H_0(x, y) + J_0(x, y). \quad (39)$$

In all generality the function $K_0(x, y)$ has a rather long expression. It takes a simple form, though, in the massless electron limit:

$$K_0(x, y) = \frac{\pi^2}{3} + 2L(x) + 2L(y/x) + \ln^2 \left(\frac{1 - y/x}{1 - x} \right), \quad (40)$$

where $L(x)$ is the Spence function defined in Appendix A. Double logarithms in (40) are exposed once infrared singularities are canceled. After the integration over the Euler angles and y , the corrected distributions for both ν_μ and $\bar{\nu}_e$, in the soft photon and massless electron limits, read:

$$\frac{d^2 N_\nu^{\text{SP}}}{dx d \cos \theta} = F_\nu^{(0)}(x) \left[1 - \frac{\alpha}{2\pi} k(x) \right], \quad (41)$$

where

$$k(x) \equiv \int dy K_0(x, y) = 2L(x) + 2\pi^2/3 + \ln^2(1 - x). \quad (42)$$

As anticipated above, the function $k(x)$ behaves as $\ln^2(1 - x)$. We see thus explicitly how the end-point singularity appears in the soft and collinear limits to the complete $\mathcal{O}(\alpha)$ corrections.

4.4 Corrected expressions

Exactly corrected neutrino distributions are obtained considering all terms of the $\mathcal{O}(\alpha)$ corrected amplitudes, eq. (25) and eq. (32). Both can be summed up after the integration of eq. (25) over $[dM d\Phi_2(P; p_e, k)]$, which simplifies real photon emission from a four body-problem to a three-body problem. The corrected energy and angular distributions are then obtained integrating $d\Phi_3(p_\mu; p_e, p_{\bar{\nu}_e}, p_{\nu_\mu})$ over the Euler angles $0 < \alpha, \gamma < 2\pi$ and over $0 < y < 1$.

QED corrections for polarized muons are calculated identically to those of unpolarized ones with the replacement $p_\mu \rightarrow p_\mu - sm_\mu$ in the amplitudes [19], where s is the muon four-spin. The integration over the phase space is slightly modified. For example, for $\bar{\nu}_e$ distribution, the Euler angles α , γ and θ are chosen to give the orientation of $\mathbf{p}_{\bar{\nu}_e}$ and the electron three-momentum, $\mathbf{P} \equiv \mathbf{p}_e$ for virtual photons and $\mathbf{P} \equiv \mathbf{p}_e + \mathbf{k}$ and $\mathbf{p}_{\bar{\nu}_e}$ with respect to a system of coordinates where the muon spin \mathbf{s} lies along the z-axis. As in the tree level expressions, θ is defined as the angle between \mathbf{s} and neutrino momentum $\mathbf{p}_{\bar{\nu}_e}$. Defining the three-vector $\mathbf{w} = \mathbf{p}_{\bar{\nu}_e} \times \mathbf{s}$, α is chosen as the angle between \mathbf{w} and the y-axis and γ between \mathbf{w} and \mathbf{P}_t , the projection of \mathbf{P} onto the plane perpendicular to $\mathbf{p}_{\bar{\nu}_e}$, see Fig. 4. With this choice, the scalar products which appear in $|M_V|^2$ and $|M_R|^2$ do not depend on γ . However, the integration over α is not trivial because (sP) and (sp_{ν_μ}) are α -dependent. We follow the results obtained in [19] for the QCD contributions.

The corrected neutrino spectra including all finite terms in the limit $m_e = 0$ [20] are:

$$\begin{aligned} \frac{d^2 N_{\nu_\mu}}{dx d \cos \theta} &= F_{\nu_\mu}^{(0)}(x) + J_{\nu_\mu}^{(0)} \mathcal{P}_\mu(x) \cos \theta - \frac{\alpha}{2\pi} (F_{\nu_\mu}^{(1)}(x) + J_{\nu_\mu}^{(1)}(x) \mathcal{P}_\mu \cos \theta) , \\ \frac{d^2 N_{\bar{\nu}_e}}{dx d \cos \theta} &= F_{\bar{\nu}_e}^{(0)}(x) + J_{\bar{\nu}_e}^{(0)}(x) \mathcal{P}_\mu \cos \theta - \frac{\alpha}{2\pi} (F_{\bar{\nu}_e}^{(1)}(x) + J_{\bar{\nu}_e}^{(1)}(x) \mathcal{P}_\mu \cos \theta) \end{aligned} \quad (43)$$

where $F_{\bar{\nu}_e, \nu_\mu}^{(0)}$ - $J_{\bar{\nu}_e, \nu_\mu}^{(0)}$ are given in eq. (5), and the one-loop corrections are given by:

$$\begin{aligned} F_{\nu_\mu}^{(1)}(x) &= F_{\nu_\mu}^{(0)}(x)k(x) + \frac{1}{6}(41 - 36x + 42x^2 - 16x^3) \ln(1 - x) \\ &+ \frac{1}{12}x(82 - 153x + 86x^2) , \\ J_{\nu_\mu}^{(1)}(x) &= J_{\nu_\mu}^{(0)}(x)k(x) + \frac{1}{6}(11 - 36x + 14x^2 - 16x^3 - 4/x) \ln(1 - x) \\ &+ \frac{1}{12}(-8 + 18x - 103x^2 + 78x^3) , \\ F_{\bar{\nu}_e}^{(1)}(x) &= F_{\bar{\nu}_e}^{(0)}(x)k(x) + (1 - x)[(5 + 8x + 8x^2) \ln(1 - x) \\ &+ \frac{1}{2}x(10 - 19x)] , \end{aligned}$$

$$\begin{aligned}
J_{\bar{\nu}_e}^{(1)}(x) &= J_{\bar{\nu}_e}^{(0)}(x)k(x) + (1-x)\left[(-3 + 12x + 8x^2 + 4/x)\ln(1-x)\right. \\
&\quad \left. + \frac{1}{2}(8 - 2x - 15x^2)\right]. \tag{44}
\end{aligned}$$

As expected from the discussion of the former subsection, the function $k(x)$ appears in eq. (44) multiplying the tree level functions $F_\nu^{(0)}$ - $J_\nu^{(0)}$. When double logarithms are exponentiated, the singular term in $\ln(1-x)$ is wash-out as well.

Fig. 5 and Fig. 7 compare the corrected and the tree level forward ν_μ and ν_e distributions, respectively. The relative correction is shown in Figs. 6, 8 for a typical range of the neutrino energy. In both cases they are of $\mathcal{O}(0.1\%)$, well below the order of the expected precision in the knowledge of the beam parameters.

In the laboratory frame, neutrino fluxes are boosted along the muon momentum direction. The formulae of the corrected distributions in that frame are given in Appendix B.

5 Muon-beam divergence

We study below the systematic uncertainty in the neutrino distributions produced by the muon beam divergence. For the sake of illustration, the quantitative results will be given for a 30 GeV unpolarized muon beam decaying in a long straight section pointing to a far detector located at 2810 km.

The natural decay angle of the forward neutrino beam in the laboratory frame is deduced from the relation between the rest and laboratory frames. In the rest frame, half of the neutrinos are emitted within the cone $\theta \leq \pi/2$. In the laboratory frame:

$$\cos \theta' = \frac{\cos \theta + \beta}{1 + \beta \cos \theta}, \tag{45}$$

where $\beta = \sqrt{1 - \gamma^{-2}}$ is the muon velocity in the laboratory frame. Therefore, half of neutrinos are emitted within the cone subtended by the decay angle $\theta' \leq 1/\gamma$. For instance, for 30 GeV muons $1/\gamma = m_\mu/E_\mu = 3$ mrad.

For the beam and baseline illustrated here, a 10 kt detector and one year of data taking [15], the statistical error on the neutrino flux is of the order of $\mathcal{O}(0.4\%)$. It is then convenient to restrain the uncertainty induced by the muon beam divergence below that level. To achieve this, the direction of the beam must be carefully monitored within the decay straight section by placing beam position monitors at its ends. The angular divergence of the parent muon beam is then small compared to the natural decay angle of the neutrino beam $\theta' \sim 1/\gamma$, see Fig. 9, aiming at present to a divergence of $\mathcal{O}(0.1/\gamma)$. It implies that the neutrino beam will be collinear, within the limits set by the decay kinematics.

In our calculations we parameterize this beam focalization by a gaussian distribution with standard deviation $\sigma \sim 0.1/\gamma$ (i.e. 0.3 mrad for 30 GeV muon beam) [14], which suppresses the flux of neutrinos as they separate from the straight direction. The divergence is introduced analytically by considering that the muon direction opens an angle α with respect to the z-axis, defined as the direction pointing towards the far detector at a distance L , see Fig. 9. The neutrino distributions in the rest frame, eq. (4), are Lorentz boosted along the z-axis. The rest-frame basis $(x, \cos \theta)$ is transformed to the lab-frame basis $(z, \cos \theta')$, where $z = E_\nu/E_\mu$ and θ' is the angle between the neutrino beam and the z-axis. Using the parameters $\beta = \sqrt{1 - \gamma^{-2}}$, the boosted distributions read:

$$\begin{aligned}
\frac{d^2 N_{\bar{\nu}_\mu, \nu_\mu}}{dz d\Omega} &= \frac{4n_\mu}{\pi L^2 m_\mu^6} E_\mu^4 z^2 (1 - \beta(\sin \varphi' \sin \alpha \sin \theta' + \cos \alpha \cos \theta')) \\
&\quad \times \left\{ \left[3m_\mu^2 - 4zE_\mu^2 (1 - \beta(\sin \varphi' \sin \alpha \sin \theta' + \cos \alpha \cos \theta')) \right] \right. \\
&\quad \left. \mp \mathcal{P}_\mu \left[m_\mu^2 - 4z(1 - \beta(\sin \varphi' \sin \alpha \sin \theta' + \cos \alpha \cos \theta')) \right] \right\}, \\
\frac{d^2 N_{\nu_e, \bar{\nu}_e}}{dz d\Omega} &= \frac{24n_\mu}{\pi L^2 m_\mu^6} E_\mu^4 z^2 (1 - \beta(\sin \varphi' \sin \alpha \sin \theta' + \cos \alpha \cos \theta')) \\
&\quad \times \left\{ \left[m_\mu^2 - 2zE_\mu^2 (1 - \beta(\sin \varphi' \sin \alpha \sin \theta' + \cos \alpha \cos \theta')) \right] \right. \\
&\quad \left. \mp \mathcal{P}_\mu \left[m_\mu^2 - 4z(1 - \beta(\sin \varphi' \sin \alpha \sin \theta' + \cos \alpha \cos \theta')) \right] \right\}. \quad (46)
\end{aligned}$$

The above expressions are integrated on α , weighted with the gaussian factor

$$\frac{e^{\frac{-\alpha^2}{2\sigma^2}}}{\sqrt{2\pi\sigma^2}}. \quad (47)$$

For unpolarized muons ($P_\mu = 0$) (for different muon polarizations we obtain similar results), it results:

$$\begin{aligned}
\frac{d^2 N_{\bar{\nu}_\mu, \nu_\mu}}{dz d\Omega} &= \frac{4n_\mu}{\pi L^2 m_\mu^6} E_\mu^4 z^2 \left\{ 3m_\mu^2 \left(1 - \beta e^{\frac{-\sigma^2}{2}} \cos \theta' \right) \right. \\
&\quad - 4zE_\mu^2 \left(1 - 2\beta e^{\frac{-\sigma^2}{2}} \cos \theta' \right. \\
&\quad \left. \left. + \beta^2 \left(\frac{1 - e^{-2\sigma^2}}{2} \right) \sin^2 \theta' \sin^2 \varphi' + \beta^2 \left(\frac{1 + e^{-2\sigma^2}}{2} \right) \cos^2 \theta' \right) \right\},
\end{aligned}$$

$$\begin{aligned}
\frac{d^2 N_{\nu_e \bar{\nu}_e}}{dz d\Omega} = & \frac{24 n_\mu}{\pi L^2 m_\mu^6} E_\mu^4 z^2 \left\{ m_\mu^2 \left(1 - \beta e^{\frac{-\sigma^2}{2}} \cos \theta' \right) \right. \\
& - 2z E_\mu^2 \left(1 - 2\beta e^{\frac{-\sigma^2}{2}} \cos \theta' \right. \\
& \left. \left. + \beta^2 \left(\frac{1 - e^{-2\sigma^2}}{2} \right) \sin^2 \theta' \sin^2 \varphi' + \beta^2 \left(\frac{1 + e^{-2\sigma^2}}{2} \right) \cos^2 \theta' \right) \right\}. \quad (48)
\end{aligned}$$

Setting $\theta' = 0$, the expression of forward neutrino fluxes reads:

$$\begin{aligned}
\frac{d^2 N_{\bar{\nu}_\mu, \nu_\mu}}{dz d\Omega} = & \frac{4 n_\mu}{\pi L^2 m_\mu^6} E_\mu^4 z^2 \left\{ 3m_\mu^2 \left(1 - \beta e^{\frac{-\sigma^2}{2}} \right) \right. \\
& \left. - 4z E_\mu^2 \left(1 - 2\beta e^{\frac{-\sigma^2}{2}} + \beta^2 \left(\frac{1 + e^{-2\sigma^2}}{2} \right) \right) \right\}, \\
\frac{d^2 N_{\nu_e \bar{\nu}_e}}{dz d\Omega} = & \frac{24 n_\mu}{\pi L^2 m_\mu^6} E_\mu^4 z^2 \left\{ m_\mu^2 \left(1 - \beta e^{\frac{-\sigma^2}{2}} \right) \right. \\
& \left. - 2z E_\mu^2 \left(1 - 2\beta e^{\frac{-\sigma^2}{2}} + \beta^2 \left(\frac{1 + e^{-2\sigma^2}}{2} \right) \right) \right\}. \quad (49)
\end{aligned}$$

Figs. 10, 11 show the numerical results for the neutrino and antineutrino spectra in a medium baseline (2810 km). We compare the distribution where the muon beam is aligned with the detector direction (no beam divergence) with the distribution where the muon-beam divergence is included. In the former, neutrino beams are averaged over an angle θ' of 0.1 mrad at the far detector [28].

Neutrino and antineutrino fluxes are shown in Figs. 12, 13 for the same localization of the detector. As it was the case for the spectra, the divergence of the beam is more important for the electron neutrino case. Our formulae predict a similar flux correction than previous numerical estimations [14]. For instance, a 10% uncertainty in the muon beam divergence would lead to a flux uncertainty of 0.3%. We obtain,

$$\frac{\frac{\Delta dN_\nu}{dE}}{\frac{dN_\nu}{dE}} \sim 0.03 \frac{\Delta \alpha}{\alpha}. \quad (50)$$

If the muon beam divergence is constrained by lattice design to be less than $0.05/\gamma$, the loss of flux will be negligible [13].

6 Conclusions

A neutrino factory from muon decay aims at a precision better than $\mathcal{O}(1\%)$ in the knowledge of the resulting intense neutrino fluxes. We have considered here the QED

corrected angular and energy flux distributions in muon decay. The tree-level electron distribution get corrections of $\mathcal{O}(1\%)$, resulting from large terms of the form $\frac{\alpha}{\pi} \ln(\frac{m_\mu}{m_e})$, that we have computed in the “leading log” approximation which turns out to be very accurate for this problem. The corresponding formulae are simple and have been presented both in the rest and laboratory frames. The radiative corrections to the neutrino distributions are also evaluated in this work, including muon polarization effects. In this case there are no leading log corrections and the exact ones must be considered (for $m_e = 0$ and $m_\nu = 0$).

Both electron and neutrino one-loop corrected distributions diverge at the upper edge of the kinematical allowed region. This results from a failure in the cancellation of infrared divergences from virtual photons by real photons. Applying the soft photon limit to the exact calculations, we have isolated the end-point divergent term for the neutrino distributions which takes the form of $\ln^2(1 - x)$. In order to control this one-loop singularity, the double logarithmic-contribution is exponentiated, encompassing the contributions from all orders of perturbation theory. All in all, the exact neutrino distributions get corrections of $\mathcal{O}(0.1\%)$, safely below the expected precision in the flux measurements.

We have also studied carefully another source of precision uncertainty: the influence of the muon beam divergence on the neutrino spectra at the far site. The challenge in designing the neutrino production section, where the muons decay, is to constrain the muon beam divergence to a value smaller than the natural cone of forward going neutrinos in the laboratory frame, ($\sim 1/\gamma$). At present, the long straight sections under discussion aim at an angular muon beam divergence of the order of $0.1/\gamma$, typically less than one mrad. We have included the angular divergence in the computation through a gaussian distribution. The induced uncertainties on the neutrino spectra turn out to be a safe $\mathcal{O}(0.1\%)$.

7 Acknowledgments

We thank M.B. Gavela, P. Hernández and A. De Rújula for their physics suggestions and useful discussions. We thank as well F.J Ynduráin for illuminating conversations. We are further indebted to A. Blondel, F. Dydak, J.J. Gómez-Cádenas. A.B acknowledges M.E.C.D for financial support by FPU grant AP2001-0521 and O.M acknowledges C.A.M for financial support by a FPI grant. The work has been partially supported by CICYT FPA2000-0980 project.

8 Note added in proof

While this paper was being written, a preprint appeared [29] where the $\mathcal{O}(\alpha)$ and $\mathcal{O}(\alpha^2)$ “leading log” corrections to the positron energy and angular distribution of muon decay

were computed. Their final results for the $\mathcal{O}(\alpha)$ corrections agree with ours.

Appendix A: QED loop corrections

A.1 Vertex correction

The vertex correction diagram, Fig. 1b, has the expression:

$$\Gamma_\sigma^b = ie^2 \int \frac{d^4k}{(2\pi)^4} \frac{1}{k^2} \gamma_\lambda \frac{p_e^\lambda - k + m_e}{(p_e - k)^2 - m_e^2} \gamma_\sigma (1 - \gamma_5) \frac{p_\mu^\lambda - k + m_\mu}{(p_\mu - k)^2 - m_\mu^2} \gamma^\lambda. \quad (51)$$

where k is the four-momentum of the virtual photon

With some algebra can be rewritten as:

$$\Gamma_\sigma^b = ie^2 \int \frac{d^4k}{(2\pi)^4} \frac{N_\sigma}{k^2 [(p_e - k)^2 - m_e^2] [(p_\mu - k)^2 - m_\mu^2]}, \quad (52)$$

where

$$\begin{aligned} N_\sigma = & 4(p_\mu p_e) \gamma_\sigma (1 - \gamma_5) - 2 [p_\mu^\lambda \gamma^\rho \gamma_\sigma (1 - \gamma_5) \\ & + \gamma_\sigma (1 - \gamma_5) \gamma^\rho p_e^\lambda] k_\rho + \gamma_\lambda \gamma_\rho \gamma_\sigma (1 - \gamma_5) \gamma_\tau \gamma^\lambda k^\rho k^\tau. \end{aligned} \quad (53)$$

The IR divergent part is contained in the first term of N_σ (independent of k) which is regularized by introducing a finite photon mass λ . The last terms (quadratic in k) is UV divergent.

After integration over the photon momentum,

$$\begin{aligned} \Gamma_\sigma^b = & -\frac{\alpha}{2\pi} [(g_{\text{IR}}^b + g_{\text{UV}}^b) \gamma_\sigma (1 - \gamma_5) + g_{\text{R}}^S \gamma_\sigma (1 + \gamma_5) \\ & + g_{\text{L}}^V p_{1\sigma} (1 - \gamma_5) + g_{\text{R}}^V p_{2\sigma} (1 + \gamma_5)], \end{aligned} \quad (54)$$

where

$$\begin{aligned} g_{\text{IR}}^b &= \coth \phi \left[\text{L} \left(\frac{2 \sinh \phi}{e^\omega - e^{-\phi}} \right) - \text{L} \left(\frac{2 \sinh \phi}{e^\phi - e^{-\omega}} \right) + (\omega - \phi) \ln \left(\frac{2 \sinh \left(\frac{\omega - \phi}{2} \right)}{2 \sinh \left(\frac{\phi + \omega}{2} \right)} \right) \right. \\ &\quad \left. + \phi \left(\omega - \ln \left(\frac{\lambda^2}{m_e^2} \right) \right) \right], \\ g_{\text{UV}}^b &= \frac{\phi \sinh \phi - \omega \sinh \omega}{2(\cosh \omega - \cosh \phi)} + \frac{1}{2} \left(\omega - \ln \left(\frac{\Lambda^2}{m_e^2} \right) \right) - \frac{3}{2}, \\ g_{\text{R}}^S &= \frac{-\phi}{\sinh \phi}, \\ g_{\text{L}}^V &= \frac{1}{2m_\mu \sinh \phi} \left[\phi - \frac{\omega \sinh \phi - \phi \sinh \omega}{\cosh \omega - \cosh \phi} \right], \\ g_{\text{R}}^V &= \frac{1}{2m_e \sinh \phi} \left[\phi + \frac{\omega \sinh \phi - \phi \sinh \omega}{\cosh \omega - \cosh \phi} \right], \end{aligned} \quad (55)$$

where, following [9],

$$\cosh \phi = \frac{(p_\mu p_e)}{m_\mu m_e} \quad e^\omega = \frac{m_\mu}{m_e}. \quad (56)$$

$L(x)$ is the Spence function

$$L(x) \equiv - \int_0^x dt \frac{\ln |1-t|}{t}. \quad (57)$$

A.2 Propagator corrections

Consider diagrams in Figs. 1c,d for $i = \mu, e$, respectively:

$$\Sigma(p_i) = ie^2 \int \frac{d^4 k}{(2\pi)^4} \frac{1}{k^2} \gamma_\lambda \frac{p'_i - k + m_i}{(p_i - k)^2 - m_i^2} \gamma^\lambda \quad (58)$$

The contribution from self-energy diagrams to the muon-electron vertex is

$$\Gamma_\sigma^{b,c} = \frac{1}{2} [Z(p_\mu) + Z(p_e)] \gamma_\sigma (1 - \gamma_5), \quad (59)$$

where

$$Z(p_i) = \left. \frac{\partial \Sigma(p_i)}{\partial p'_i} \right|_{p'_i = m_i}. \quad (60)$$

$Z(p_i)$ is both UV and IR divergent:

$$Z(p_i) = -\frac{\alpha}{2\pi} (h_{\text{IR}}^{(i)} + h_{\text{UV}}^{(i)}), \quad (61)$$

where the functions “h” read

$$h_{\text{UV}}^{(i)} = \frac{3}{2} - \frac{1}{2} \ln \left(\frac{\Lambda^2}{m_i^2} \right), \quad (62)$$

$$h_{\text{IR}}^{(i)} = 2 + \ln \left(\frac{\lambda^2}{m_i^2} \right). \quad (63)$$

(64)

Adding both muon and electron self-energies, eq. (59) has the following expression:

$$\Gamma_\sigma^{c,d} = -\frac{\alpha}{2\pi} (h_{\text{UV}}^{c,d} + h_{\text{IR}}^{c,d}), \quad (65)$$

where, now,

$$h_{\text{UV}}^{c,d} = -\frac{1}{2} \left(\omega - \ln \left(\frac{\Lambda^2}{m_e^2} \right) \right) + \frac{3}{2}, \quad (66)$$

$$h_{\text{IR}}^{c,d} = \left(\omega - \ln \left(\frac{\lambda^2}{m_e^2} \right) \right) + 2. \quad (67)$$

Adding eq. (55) and eq. (66) the UV divergences are exactly cancelled. The IR divergences, when combined with eq. (54) gives rise to the term

$$\begin{aligned} g_L^S &= -\coth \phi \left[\phi - L \left(\frac{2 \sinh \phi}{e^\omega - e^{-\phi}} \right) + L \left(\frac{2 \sinh \phi}{e^\phi - e^{-\omega}} \right) - (\omega - \phi) \ln \left(\frac{2 \sinh \left(\frac{\omega - \phi}{2} \right)}{2 \sinh \left(\frac{\phi + \omega}{2} \right)} \right) \right], \\ &+ \frac{\phi \sinh \phi - \omega \sinh \omega}{2(\cosh \omega - \cosh \phi)} + 2 - (1 - \phi \coth \phi) \left(\omega - \ln \left(\frac{\lambda^2}{m_e^2} \right) \right). \end{aligned} \quad (68)$$

which multiplies $\gamma_\sigma(1 - \gamma_5)$ in the $\mathcal{O}(\alpha)$ correction to $\mu - e$ vertex of eq. (23).

Appendix B: QED corrected distributions in the laboratory frame

In order to obtain the neutrino distributions in the laboratory frame, a Lorentz boost is performed in the direction of the muon velocity towards the detector at a distance L . The rest-frame basis $(x, \cos \theta)$ is transformed to the lab-frame basis $(z, \cos \theta')$, where $z = E_\nu/E_\mu$ is the scaled energy at the laboratory frame and θ' is the angle between the neutrino beam and the direction of the muon beam [28]. The muon beam divergence is set to zero. Using the parameters $\gamma = E_\mu/m_\mu$ and $\beta = \sqrt{1 - \gamma^{-2}}$, the boosted distributions read:

$$\begin{aligned} \frac{d^2 N_{\nu_\mu}}{dz d \cos \theta'} &= F_{\nu_\mu}^{(0)}(z, \theta') + \mathcal{P}_\mu J_{\nu_\mu}^{(0)}(z, \theta') \cos \theta' \\ &\quad - \frac{\alpha}{2\pi} \left[\tilde{F}_{\nu_\mu}^{(1)}(z, \theta') + \mathcal{P}_\mu \tilde{J}_{\nu_\mu}^{(1)}(z, \theta') \cos \theta' \right], \end{aligned} \quad (69)$$

$$\begin{aligned} \frac{d^2 N_{\bar{\nu}_e}}{dz d \cos \theta'} &= F_{\bar{\nu}_e}^{(0)}(z, \theta') + \mathcal{P}_\mu J_{\bar{\nu}_e}^{(0)}(z, \theta') \cos \theta' nn \\ &\quad - \frac{\alpha}{2\pi} \left[\tilde{F}_{\bar{\nu}_e}^{(1)}(z, \theta') + \mathcal{P}_\mu \tilde{J}_{\bar{\nu}_e}^{(1)}(z, \theta') \cos \theta' \right], \end{aligned} \quad (70)$$

where

$$\begin{aligned} F_{\nu_\mu}^{(0)}(z, \theta') &= 8 \frac{E_\mu^4}{m_\mu^6} z^2 (1 - \beta \cos \theta') (3m_\mu^2 - 4E_\mu^2 z (1 - \beta \cos \theta')), \\ J_{\nu_\mu}^{(0)}(z, \theta') &= 8 \frac{E_\mu^4}{m_\mu^6} z^2 (1 - \beta \cos \theta') (m_\mu^2 - 4E_\mu^2 z (1 - \beta \cos \theta')), \\ F_{\bar{\nu}_e}^{(0)}(z, \theta') &= 48 \frac{E_\mu^4}{m_\mu^6} z^2 (1 - \beta \cos \theta') (m_\mu^2 - 2E_\mu^2 z (1 - \beta \cos \theta')), \\ J_{\bar{\nu}_e}^{(0)}(z, \theta') &= 48 \frac{E_\mu^4}{m_\mu^6} z^2 (1 - \beta \cos \theta') (m_\mu^2 - 2E_\mu^2 z (1 - \beta \cos \theta')), \\ F_{\nu_\mu}^{(1)}(z, \theta') &= F_{\nu_\mu}^{(0)}(z, \theta') k(z, \theta') + \frac{1}{3(1 - \beta \cos \theta')} \left\{ \begin{aligned} & \left[41 - 36 (2\gamma^2 z (1 - \beta \cos \theta')) \right. \\ & + 42 (2\gamma^2 z (1 - \beta \cos \theta'))^2 - 16 (2\gamma^2 z (1 - \beta \cos \theta'))^3 \Big] \\ & \times \ln (1 - 2\gamma^2 z (1 - \beta \cos \theta')) \\ & + \frac{1}{2} (2\gamma^2 z (1 - \beta \cos \theta')) \left[82 - 153 (2\gamma^2 z (1 - \beta \cos \theta')) \right. \\ & \left. \left. + 86 (2\gamma^2 z (1 - \beta \cos \theta'))^2 \right] \end{aligned} \right\}, \end{aligned}$$

$$\begin{aligned}
J_{\nu_\mu}^{(1)}(z, \theta') &= J_{\nu_\mu}^{(0)}(z, \theta')k(z, \theta') + \frac{1}{3(1 - \beta \cos \theta')} \left\{ \left[11 - 36 \left(2\gamma^2 z (1 - \beta \cos \theta') \right) \right. \right. \\
&+ 14 \left(2\gamma^2 z (1 - \beta \cos \theta') \right)^2 - 16 \left(2\gamma^2 z (1 - \beta \cos \theta') \right)^3 \\
&+ 4 \left(2\gamma^2 z (1 - \beta \cos \theta') \right)^{-1} \left. \right] \times \ln \left(1 - 2\gamma^2 z (1 - \beta \cos \theta') \right) \\
&+ \frac{1}{2} \left[-8 + 18 \left(2\gamma^2 z (1 - \beta \cos \theta') \right) \right. \\
&\left. \left. - 103 \left(2\gamma^2 z (1 - \beta \cos \theta') \right)^2 + 78 \left(2\gamma^2 z (1 - \beta \cos \theta') \right)^3 \right] \right\},
\end{aligned}$$

$$\begin{aligned}
F_{\bar{\nu}_e}^{(1)}(z, \theta') &= F_{\nu_e}^{(0)}(z, \theta')k(z, \theta') + \frac{2 \left(1 - 2\gamma^2 z (1 - \beta \cos \theta') \right)}{(1 - \beta \cos \theta')} \\
&\times \left\{ \left[5 + 8 \left(2\gamma^2 z (1 - \beta \cos \theta') \right) \right. \right. \\
&+ 8 \left(2\gamma^2 z (1 - \beta \cos \theta') \right)^2 \left. \right] \ln \left(1 - 2\gamma^2 z (1 - \beta \cos \theta') \right) \\
&+ \frac{1}{2} \left(2\gamma^2 z (1 - \beta \cos \theta') \right) \left[10 - 19 \left(2\gamma^2 z (1 - \beta \cos \theta') \right) \right] \left. \right\},
\end{aligned}$$

$$\begin{aligned}
J_{\bar{\nu}_e}^{(1)}(z, \theta') &= J_{\nu_e}^{(0)}(z, \theta')k(z, \theta') + \frac{2 \left(1 - 2\gamma^2 z (1 - \beta \cos \theta') \right)}{(1 - \beta \cos \theta')} \\
&\times \left\{ \left[-3 + 12 \left(2\gamma^2 z (1 - \beta \cos \theta') \right) + 8 \left(2\gamma^2 z (1 - \beta \cos \theta') \right)^2 \right. \right. \\
&+ 4 \left(2\gamma^2 z (1 - \beta \cos \theta') \right)^{-1} \left. \right] \ln \left(1 - 2\gamma^2 z (1 - \beta \cos \theta') \right) \\
&+ \frac{1}{2} \left[8 - 2 \left(2\gamma^2 z (1 - \beta \cos \theta') \right) - 15 \left(2\gamma^2 z (1 - \beta \cos \theta') \right)^2 \right] \left. \right\},
\end{aligned}$$

$$k(z, \theta') = \ln^2 \left(1 - 2\gamma^2 z (1 - \beta \cos \theta') \right) + 2L \left(2\gamma^2 z (1 - \beta \cos \theta') \right) + \frac{2\pi^2}{3} \quad (71)$$

Appendix C: QED corrected e^- distributions in the laboratory frame

The “leading log” corrected distributions in eq. (17) are boosted to the lab frame, using the same parameterization than Appendix B:

$$\begin{aligned} \frac{d^2N_e}{dzd\cos\theta'} &= \left\{ F_e^{(0)}(z, \theta') + \mathcal{P}_\mu J_e^{(0)}(z, \theta') \cos\theta' \right\} \\ &\times \left(1 - \frac{\alpha}{2\pi} \psi(z, \theta') \right), \end{aligned} \quad (72)$$

where

$$\begin{aligned} F_e^{(0)}(z, \theta') &= 8 \frac{E_\mu^4}{m_\mu^6} z^2 (1 - \beta \cos\theta') (3m_\mu^2 - 4E_\mu^2 z (1 - \beta \cos\theta')), \\ J_e^{(0)}(z, \theta') &= 8 \frac{E_\mu^4}{m_\mu^6} z^2 (1 - \beta \cos\theta') (m_\mu^2 - 4E_\mu^2 z (1 - \beta \cos\theta')), \end{aligned} \quad (73)$$

The “leading log” correction is contained in

$$\begin{aligned} \psi(z, \theta') &= 2 \ln \left(\frac{m_\mu}{m_e^2} \right) \left[\ln \left(\frac{(1 - 2\gamma^2 z (1 - \beta \cos\theta'))}{(2\gamma^2 z (1 - \beta \cos\theta'))} \right) \right. \\ &+ \frac{5}{6} + 2 \left(2\gamma^2 z (1 - \beta \cos\theta') \right) - 4 \left(2\gamma^2 z (1 - \beta \cos\theta') \right)^2 \\ &\left. + \frac{8 \left(2\gamma^2 z (1 - \beta \cos\theta') \right)^3}{3} \right]. \end{aligned} \quad (74)$$

We will also boost the $\mathcal{O}(\alpha)$ exactly corrected electron distributions, computed in [9]. In the muon rest frame they have the following expression:

$$\begin{aligned} \frac{d^2N_e}{dxd\cos\theta} &= F_e^{(0)}(x) + \mathcal{P}_\mu J_e^{(0)}(x) \cos\theta \\ &- \frac{\alpha}{2\pi} \left[\tilde{F}_{\nu_\mu}^{(1)}(x) + \mathcal{P}_\mu \tilde{J}_e^{(1)}(x) \cos\theta \right], \end{aligned} \quad (75)$$

where $F_e^{(0)}(x)$ and $J_e^{(0)}(x)$ are the tree level results, and

$$\begin{aligned} F_e^{(1)}(x) &= 2F_e^{(0)}(x) h(x) + 6(1 - x)x^2 \ln(x) \\ &+ \frac{(1 - x)}{3} \left\{ (5 + 17x - 34x^2) \left[\ln \left(\frac{m_\mu}{m_e} \right) + \ln(x) \right] - 22x + 34x^2 \right\}, \end{aligned}$$

$$\begin{aligned}
J_e^{(1)}(x) &= 2J_e^{(0)}(x)h(x) + 2(1-3x)x^2\ln(1-x) \\
&- \frac{(1-x)}{3}\left\{\left(1+x+34x^2\right)\left[\ln\left(\frac{m_\mu}{m_e}\right) + \ln(x)\right] + 3 - 7x - 32x^2\right. \\
&+ \left.4\frac{(1-x)^2}{x}\ln(1-x)\right\}, \\
h(x) &= 2L(x) - \frac{\pi^2}{3} - 2 + \ln\left(\frac{m_\mu}{m_e}\right)\left[\frac{3}{2} + 2\ln\left(\frac{1-x}{x}\right)\right] \\
&- 2\ln^2(x) + \ln(x) + 3\ln(x)\ln(1-x) - \ln(1-x) - \frac{\ln(1-x)}{x}. \quad (76)
\end{aligned}$$

After the boost, the corrected electron distribution has the form:

$$\begin{aligned}
\frac{d^2N_e}{dzd\cos\theta'} &= F_e^{(0)}(z, \theta') + \mathcal{P}_\mu J_e^{(0)}(z, \theta')\cos\theta' \\
&- \frac{\alpha}{2\pi}\left[\tilde{F}_{\nu_\mu}^{(1)}(z, \theta') + \mathcal{P}_\mu \tilde{J}_e^{(1)}(z, \theta')\cos\theta'\right], \quad (77)
\end{aligned}$$

where $F_e^{(0)}(z, \theta')$, $J_e^{(0)}(z, \theta')$ are given in eq. (73)

$$\begin{aligned}
F_e^{(1)}(z, \theta') &= 2F_e^{(0)}(z, \theta')h(z, \theta') \\
&+ \frac{12\left(1-2\gamma^2z(1-\beta\cos\theta')\right)^2}{(2\gamma^2z(1-\beta\cos\theta'))}(1-\beta\cos\theta') \\
&\times \ln\left(2\gamma^2z(1-\beta\cos\theta')\right) \\
&+ \frac{2\left(1-2\gamma^2z(1-\beta\cos\theta')\right)}{3(1-\beta\cos\theta')}\left\{\left(5+17\left(2\gamma^2z(1-\beta\cos\theta')\right)\right.\right. \\
&\left.\left.-34\left(2\gamma^2z(1-\beta\cos\theta')\right)^2\right)\left[\ln\left(\frac{m_\mu}{m_e}\right) + \ln\left(2\gamma^2z(1-\beta\cos\theta')\right)\right]\right. \\
&\left.-22\left(2\gamma^2z(1-\beta\cos\theta')\right) + 34\left(2\gamma^2z(1-\beta\cos\theta')\right)^2\right\},
\end{aligned}$$

$$\begin{aligned}
J_e^{(1)}(z, \theta') &= 2J_e^{(0)}(z, \theta') h(z, \theta') \\
&+ \frac{4 \left(1 - 3 \left(2\gamma^2 z (1 - \beta \cos \theta') \right) \right) \left(2\gamma^2 z (1 - \beta \cos \theta') \right)^2 \ln \left(2\gamma^2 z (1 - \beta \cos \theta') \right)}{(1 - \beta \cos \theta')} \\
&- \frac{2 \left(1 - \left(2\gamma^2 z (1 - \beta \cos \theta') \right) \right)}{3(1 - \beta \cos \theta')} \left\{ \left(1 + \left(2\gamma^2 z (1 - \beta \cos \theta') \right) \right) \right. \\
&+ 34 \left(2\gamma^2 z (1 - \beta \cos \theta') \right)^2 \left[\ln \left(\frac{m_\mu}{m_e} \right) + \ln \left(2\gamma^2 z (1 - \beta \cos \theta') \right) \right] \\
&+ 3 - 7 \left(2\gamma^2 z (1 - \beta \cos \theta') \right) - 32 \left(2\gamma^2 z (1 - \beta \cos \theta') \right)^2 \\
&+ \left. 4 \frac{\left(1 - 2\gamma^2 z (1 - \beta \cos \theta') \right)^2}{(2\gamma^2 z (1 - \beta \cos \theta'))} \ln \left(1 - 2\gamma^2 z (1 - \beta \cos \theta') \right) \right\}, \\
h(z, \theta') &= 2L \left(2\gamma^2 z (1 - \beta \cos \theta') \right) - 2 - \frac{\pi^2}{3} \\
&+ \ln \left(\frac{m_\mu}{m_e} \right) \left[\frac{3}{2} + 2 \ln \left(1 - 2\gamma^2 z (1 - \beta \cos \theta') \right) \right. \\
&- 2 \ln \left(2\gamma^2 z (1 - \beta \cos \theta') \right) \left. \right] \\
&- 2 \ln^2 \left(2\gamma^2 z (1 - \beta \cos \theta') \right) + \ln \left(2\gamma^2 z (1 - \beta \cos \theta') \right) \\
&+ 3 \ln \left(2\gamma^2 z (1 - \beta \cos \theta') \right) \ln \left(1 - 2\gamma^2 z (1 - \beta \cos \theta') \right) \\
&- \left(1 + \left(2\gamma^2 z (1 - \beta \cos \theta') \right)^{-1} \right) \ln \left(1 - 2\gamma^2 z (1 - \beta \cos \theta') \right). \tag{78}
\end{aligned}$$

References

- [1] Y. Fukuda *et al.* [SuperKamiokande Collaboration], Phys. Rev. Lett. **82** (1999) 2644
- [2] J. N. Bahcall, P. I. Krastev and A. Y. Smirnov, JHEP **0105** (2001) 015
- [3] S. H. Ahn *et al.* [K2K Collaboration], Phys. Lett. B **511**, 178 (2001),
MINOS Collaboration <http://www-numi.fnal.gov:8875/>,
A. G. Cocco [OPERA Collaboration], Nucl. Phys. Proc. Suppl. **85**, 125 (2000).
- [4] T. Adams *et al.*, in *Proc. of the APS/DPF/DPB Summer Study on the Future of Particle Physics (Snowmass 2001)* ed. R. Davidson and C. Quigg, arXiv:hep-ph/0111030.
- [5] V. D. Barger *et al.*, hep-ph/0103052.
- [6] J. J. Gomez-Cadenas *et al.* [CERN working group on Super Beams Collaboration]
hep-ph/0105297.
- [7] S. Geer, Phys. Rev. D **57** (1998) 6989 [Erratum-ibid. D **59** (1998)]
- [8] A. Blondel *et al.*, Nucl. Instrum. Meth. A **451** (2000) 102.
- [9] R.J. Finkelstein, R. E. Behrends and A. Sirlin, *Phys. Rev.* 101 (1956) 866;
S. Berman, *Phys. Rev.* 112 (1958) 267;
T. Kinoshita and A. Sirlin, *Phys. Rev.* 113 (1959) 1652.
- [10] A. Blondel *et al.*, “Energy calibration by spin precession”,
Report. CERN 99-02 (1999).
- [11] A. Blondel, Nucl. Instrum. Meth. A **451** (2000) 131.// A. Blondel, M. Donega
and S. Gilardoni, CERN-NUFACT-NOTE-078.
- [12] C. Greub, D. Wyler and W. Petscher, Phys. Lett. B **324** (1994) 109 [Erratum-ibid.
B **329** (1994) 526]
- [13] I. M. Papadopoulos, Nucl. Instrum. Meth. A 451, 138 (2000).
- [14] C. Crisan and S. Geer, report FERMILAB-TM-2001.
- [15] S. Geer, C. Johnstone and D. Neuffer, FERMILAB-Pub-99/121.
- [16] T. K. Gaisser, “*Cosmic Rays and Particle Physics*”, Cambridge University Press,
1990.
- [17] D. E. Groom *et al.* [Particle Data Group Collaboration],
Eur. Phys. J. C **15** (2000) 1.

- [18] M. Jeżabek and J. H. Kühn, Nucl. Phys. **B320** (1989) 20.
- [19] A. Czarnecki, M. Jeżabek and J.H. Kühn, Nucl. Phys.**B351** (1991) 70.
- [20] A. Czarnecki, M. Jeżabek, Nucl. Phys. **B427** (1994) 3
- [21] A. Czarnecki, M. Jeżabek and J.H. Kühn, Phys. Lett. **B346** (1995) 335.
- [22] T. Kinoshita, J.Math.Phys. **3** (1962) 650;
T.D. Lee, M. Nauenberg, Phys. Rev **133** (1964) B1549.
- [23] L. Matsson, Nucl.Phys. **B12** (1969) 647;
D.A. Ross, Nuovo Cim. **10A** (1972) 475;
A.M. Sachs and A.Sirlin, “*Muon physics*”, ed.V.H.Hughes,1975.
- [24] D. Yennie, S. Frautschi and H.Suura, Ann.Phys. **13** (1961) 379;
S. Weinberg, Phys. Rev **140** (1965) B516.
- [25] F. J. Yndurain, “*The Theory of Quarks and Gluon Interactions*”,
Springer-Verlag, 1983.
- [26] A. De Rujula, R. Petronzio and A. Savoy-Navarro, Nucl. Phys. B **154**, 394 (1979)
- [27] M. E. Peskin, “*An Introduction to Quantum Field Theory*”, Perseus Books, 1995.
- [28] A. Cervera, A. Donini, M. B. Gavela, J. J. Gomez Cadenas, P. Hernandez, O. Mena
and S. Rigolin, Nucl. Phys. B **579** (2000) 17, [Erratum-ibid. B **593** (2000) 731]
- [29] A. Arbuzov, A. Czarnecki and A. Gaponenko, hep-ph/0202102.

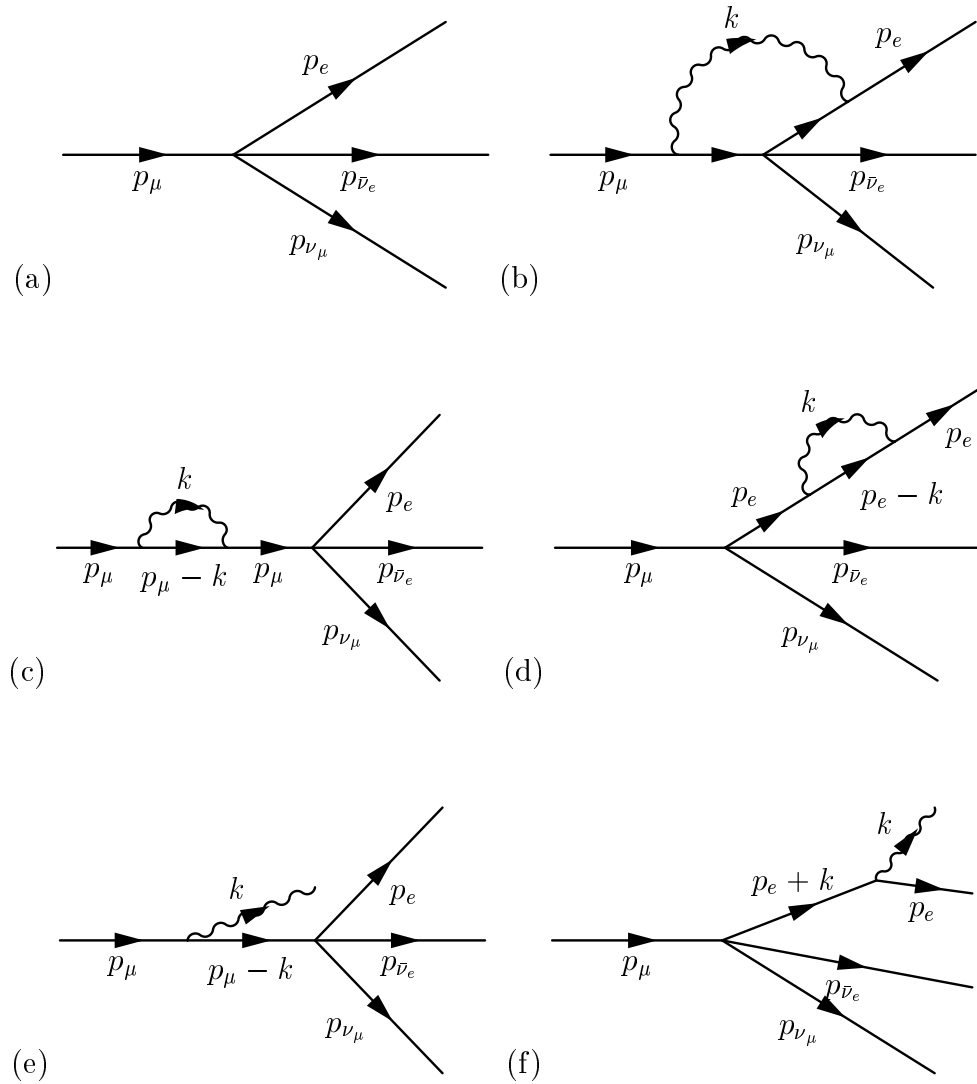


Figure 1: QED Radiative corrections to muon decay: (a) Tree level, (b) Vertex correction, (c) Muon propagator correction, (d) Electron propagator correction, (e) Muon leg bremsstrahlung, (f) Electron leg bremsstrahlung

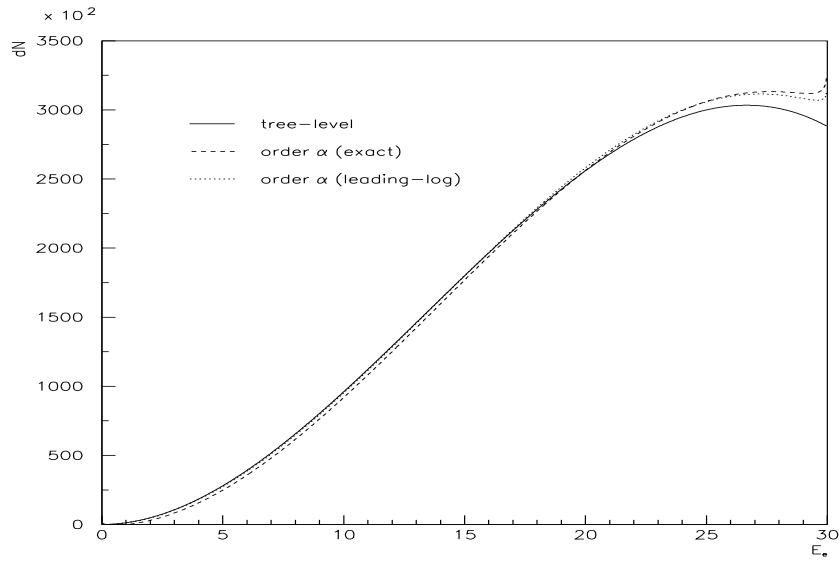


Figure 2: Electron energy distribution in the forward direction for $E_\mu = 30$ GeV and $\mathcal{P}_\mu = 0.2$. The tree level results (solid line) are shown together with the “leading log” (dotted line) and exact one-loop corrected ones (dashed-line)

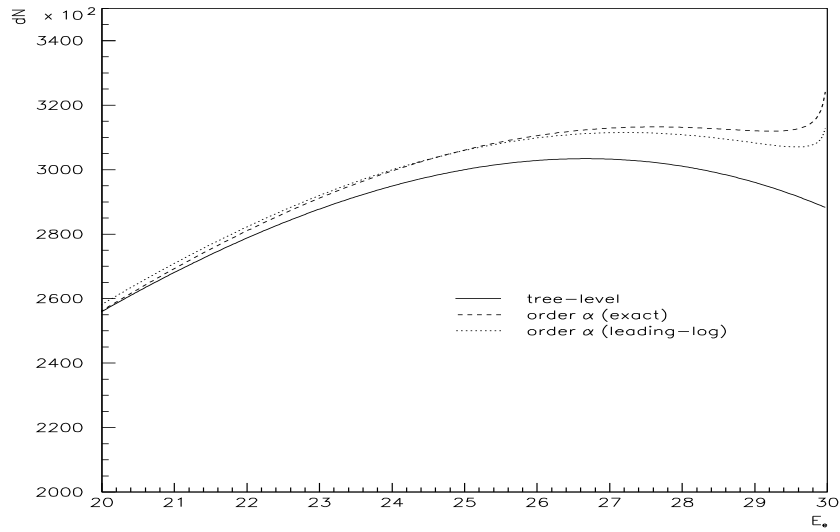


Figure 3: End-point behavior of Fig. 2.

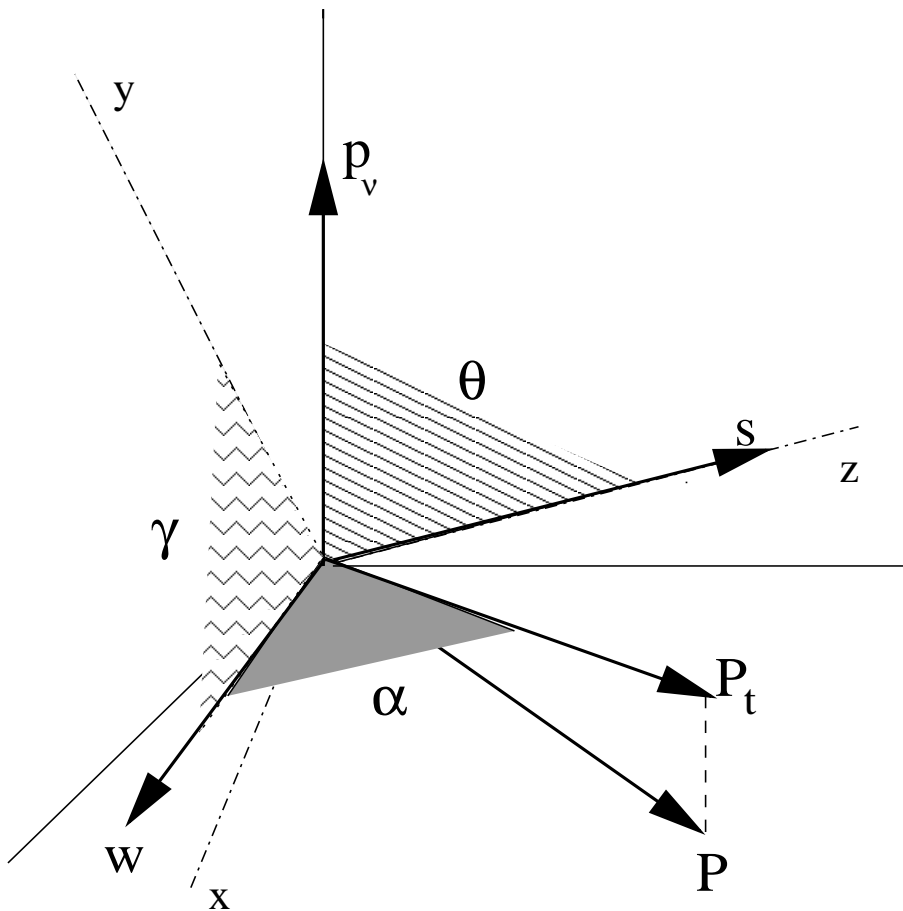


Figure 4: The three Euler angles α , γ and θ which describe the orientation of the outgoing neutrino with momentum \mathbf{p}_ν and the electron with momentum \mathbf{P} with respect to the muon spin \mathbf{s} directed along the z -axis

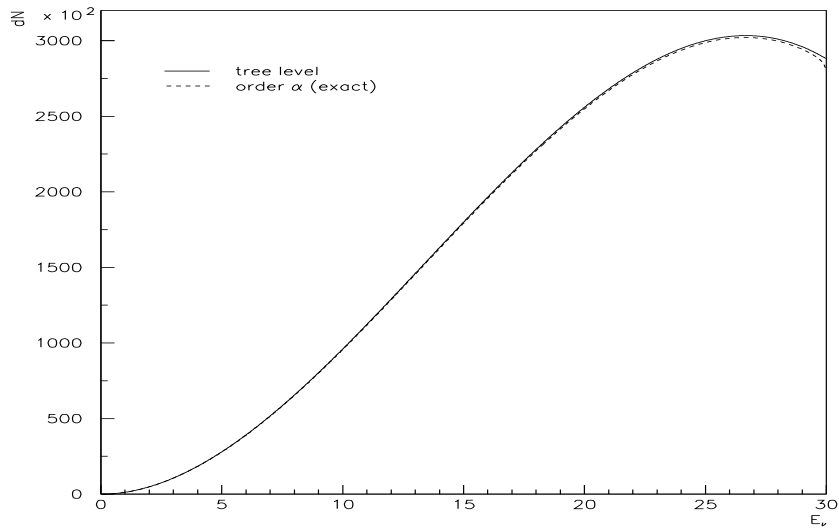


Figure 5: Zeroth order and $\mathcal{O}(\alpha)$ corrected ν_μ forward distributions. Parent muon parameters as in Fig. 2.

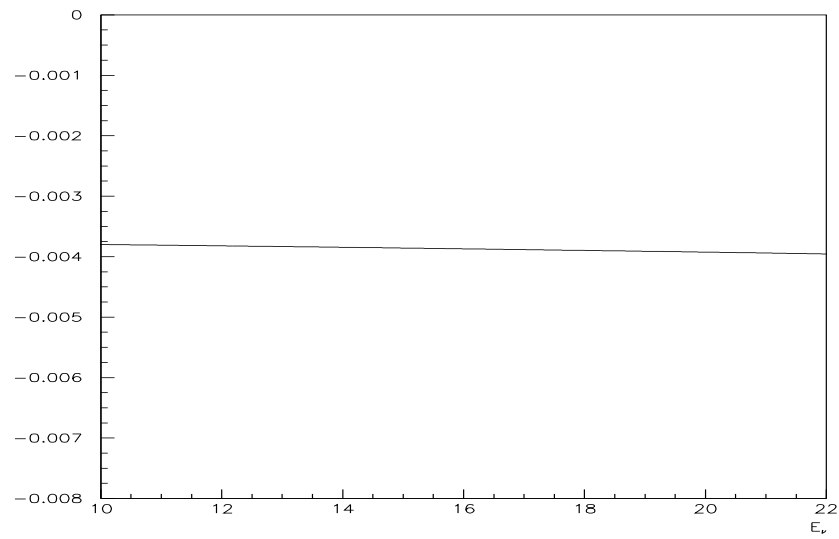


Figure 6: $\mathcal{O}(\alpha)$ relative correction to the ν_μ distribution in Fig. 5 for a typical range of E_{ν_μ} .

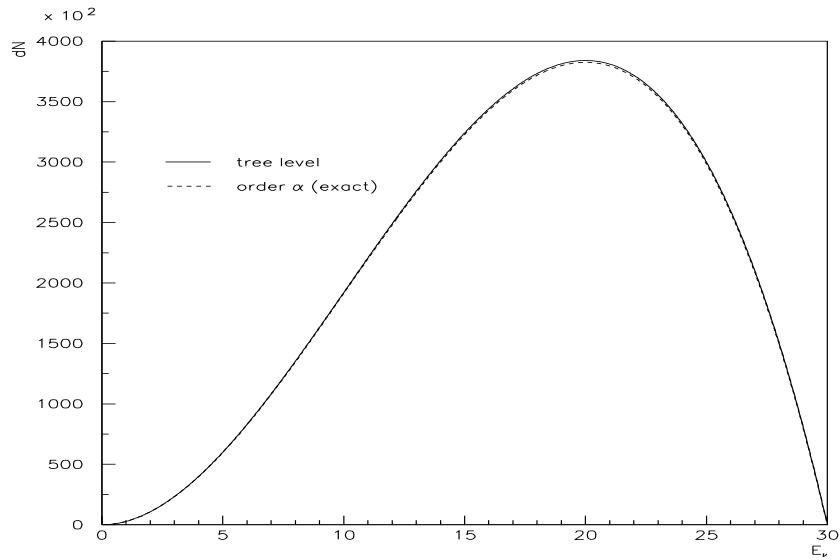


Figure 7: Zeroth order and $\mathcal{O}(\alpha)$ corrected $\bar{\nu}_e$ forward distributions. Parent muon parameters as in Fig. 2.

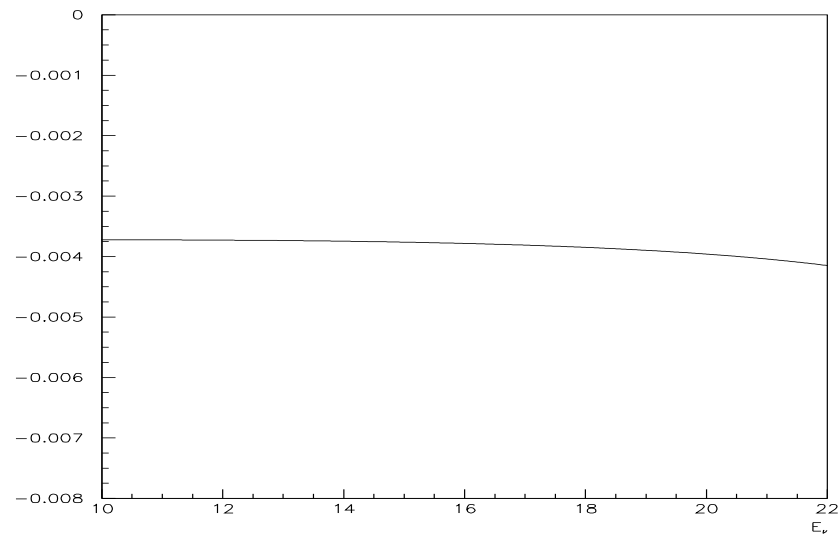


Figure 8: $\mathcal{O}(\alpha)$ relative correction to $\bar{\nu}_e$ distribution in Fig. 7 for a typical range of $E_{\bar{\nu}_e}$.

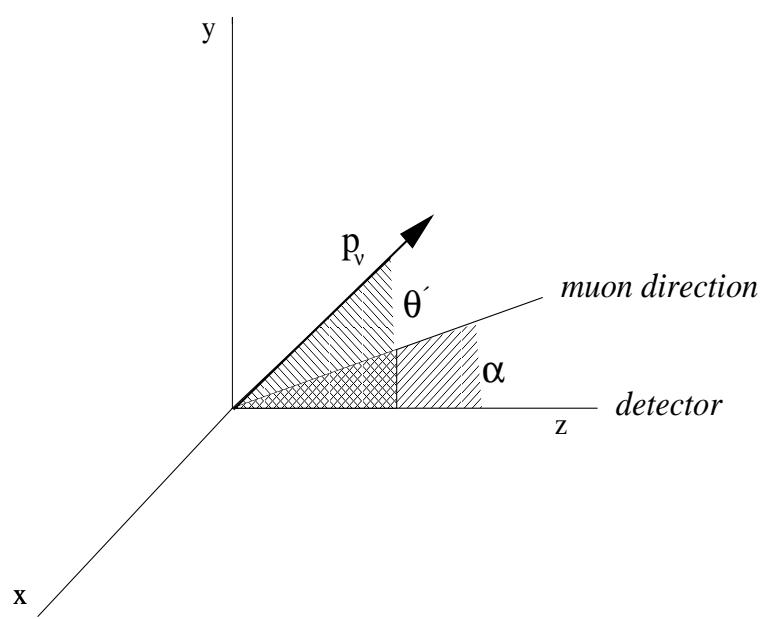


Figure 9: Muon divergence in the laboratory frame

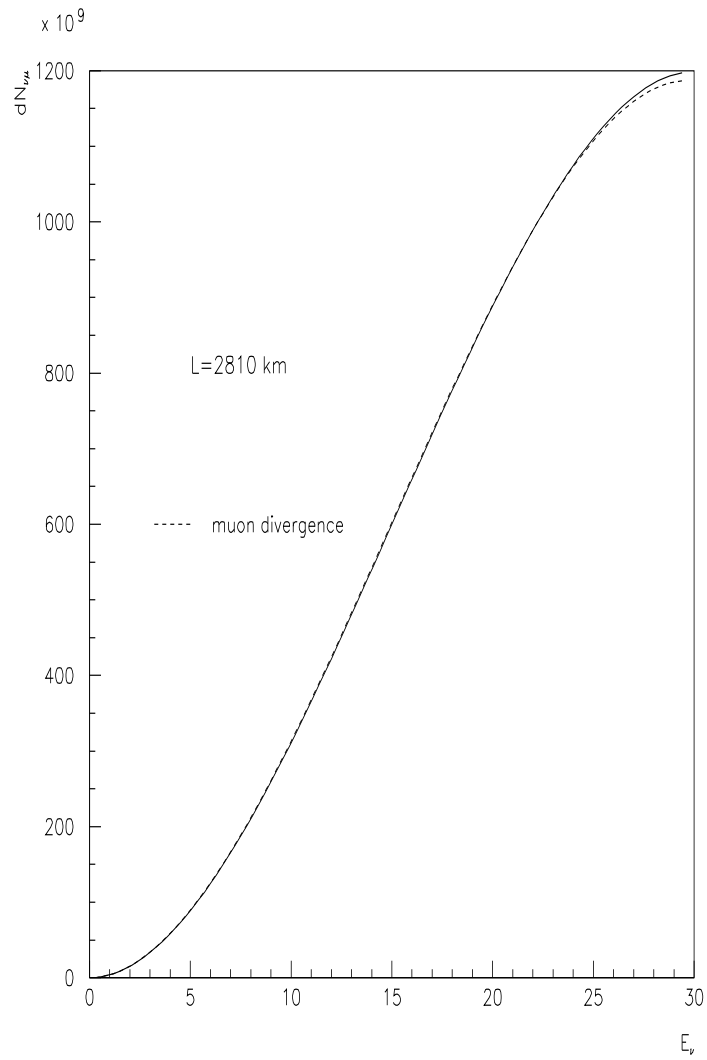


Figure 10: ν_μ and $\bar{\nu}_\mu$ differential distributions. The solid lines represent the spectra obtained by averaging over an angular divergence of 0.1 mrad and the dashed lines the spectra including muon beam divergence. The distributions are plotted in the forward direction $\cos\theta = 0$ pointing towards a detector located 2810 km from a the neutrino source of unpolarized positive or negative muons circulating in the storage ring with energies of 30 GeV.

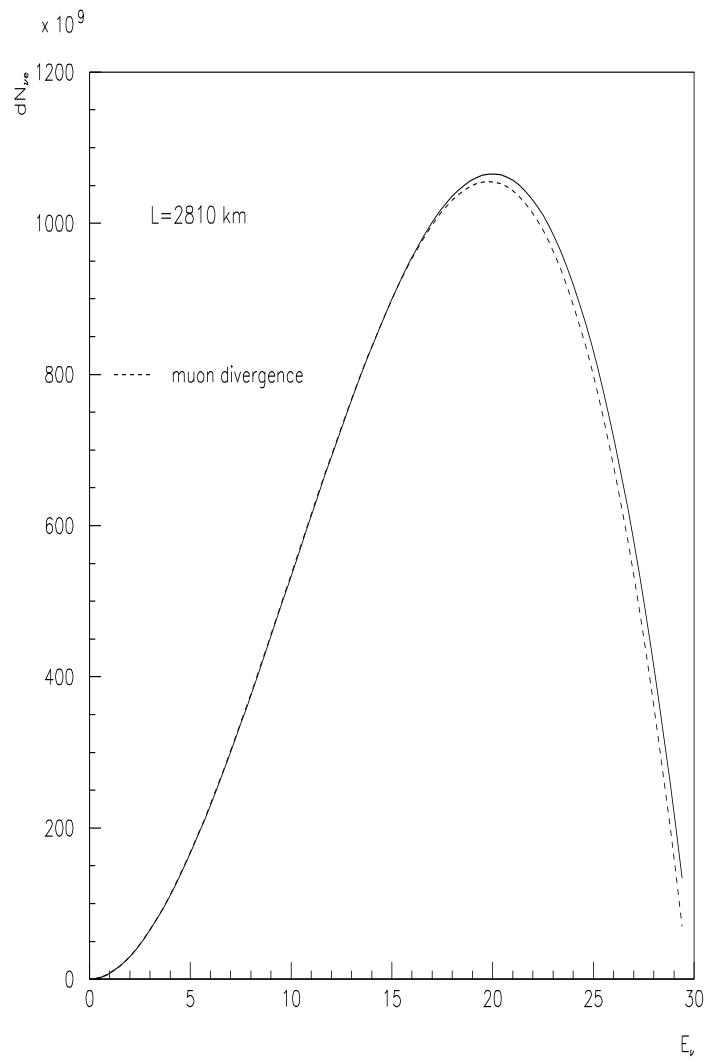


Figure 11: ν_e and $\bar{\nu}_e$ differential distributions. The solid lines represent the spectra obtained by averaging over an angular divergence of 0.1 mrad and the dashed lines the spectra including muon beam divergence. The distributions are plotted with the same parameters as of fig(10).

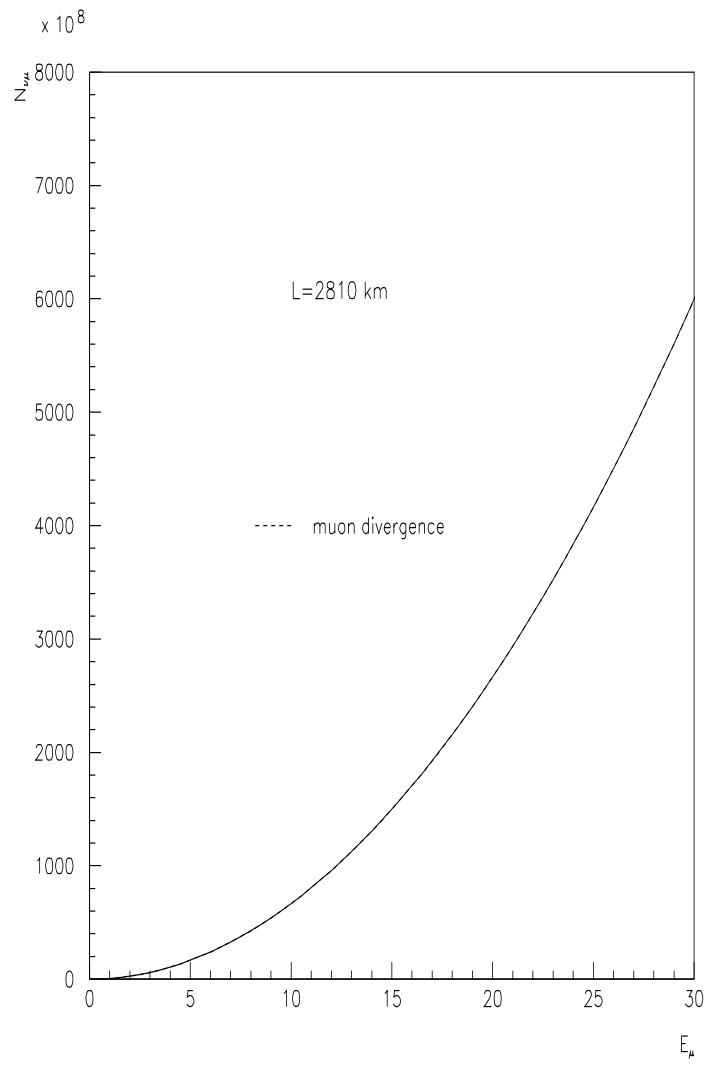


Figure 12: ν_μ and $\bar{\nu}_\mu$ fluxes. The solid lines represent the spectra obtained by averaging over an angular divergence of 0.1 mrad and the dashed lines the spectra including muon beam divergence. The distributions are plotted with the same parameters as of fig(10).

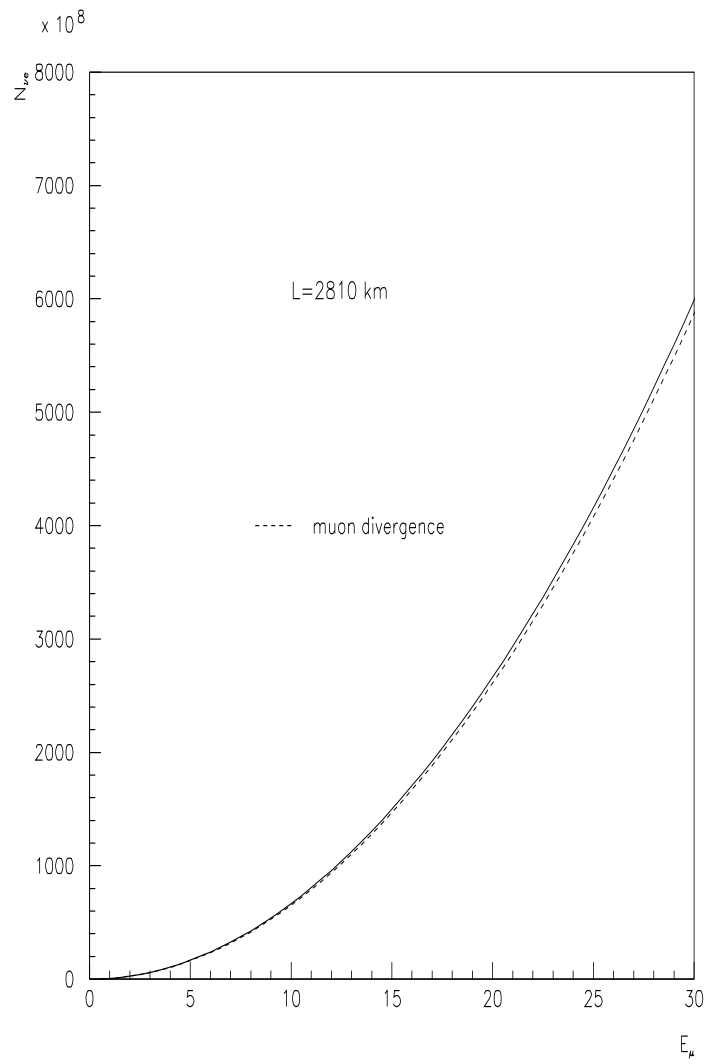


Figure 13: ν_e and $\bar{\nu}_e$ fluxes. The solid lines represent the spectra obtained by averaging over an angular divergence of 0.1 mrad and the dashed lines the spectra including muon beam divergence. The distributions are plotted with the same parameters as of fig(10).